Evidence for a Trajectory of Hydrolytic Reactions brought about by [L_3Zn-OH] Species

Michael Rombach,[a] Carsten Maurer,[a] Karl Weis,[a] Egbert Keller,[b] and Heinrich Vahrenkamp*[a]

Abstract: A kinetic study has been performed on the hydrolytic cleavage of various triorganophosphates $PO(OR)_2(OR')$ by three pyrazolylborate–zinc hydroxide complexes [Tp′Zn–OH] to form [Tp′Zn–$OPO(OR)_2$] and HOR′. The nature of the reactions (first order both in the zinc complex and the phosphate) and the strongly negative activation entropies (-54 to $-126\ J\,mol^{-1}\,K^{-1}$) indicate an intimate association of the Zn–OH and P=O functions in the rate-determining step. Some ester cleavages by [Tp′Zn–OH] show the same kinetic pattern and similar activation parameters. The observations are in accord with a four-center arrangement (ZnOPO or ZnOCO) in the activated complex, that is, the hybrid mechanism discussed for zinc enzyme as well as zinc complex catalyzed hydrolyses. A trajectory for reactions passing through this intermediate has been constructed with the Bürgi–Dunitz structure correlation method, based on the geometries of 30 [Tp′Zn(X)(Y)] species with truly five-coordinate zinc centers. Its first step is the approach of the substrate's oxygen atom to the tetrahedral L_3Zn-OH species along the axis of a trigonal bipyramid. In the resulting four-center intermediate with five-coordinate zinc a Berry pseudorotation describes the synchronous formation of the Zn–O(substrate) and breaking of the Zn–O(OH) bonds. The concluding step in the coordination sphere of zinc is the expulsion of the former OH oxygen, now part of the substrate, again along the axis of a trigonal bipyramid. This mechanism, which is applicable to phosphate as well as to ester, amide, and carbon dioxide hydrolysis, is in accord with theoretical models of carbonic anhydrase action.

Keywords: bioinorganic chemistry · hydrolyses · kinetics · reaction mechanisms · structure correlations · zinc

Introduction

Nature has chosen zinc as the most prominent inorganic constituent of hydrolytic enzymes, its qualification being its coordinative flexibility and redox inertness. Hence there is ample justification to study zinc complexes as enzyme models, and many publications and several reviews[1–6] have dealt with this topic. As it became clear that the catalytically active species is a covalently bound Zn–OH unit existing near neutral pH[7–12] the model chemistry focused on zinc complexes, preferably of tridentate ligands, bearing one OH_2 or OH ligand. It is difficult, however, to isolate mononuclear Zn–OH complexes, and to our knowledge only eight such complexes have been obtained in a pure form,[13–19] six of which are of the type [Tp′Zn–OH], bearing substituted pyrazolylborate (Tp′) ligands.

Indirect evidence, mostly from rate versus pH profiles, for the involvement of Zn–OH species was gained from studies of zinc-complex-mediated hydrolysis reactions. The first of such studies involved the acetalization of acetaldehyde.[20] Investigations of CO_2 hydration,[20–24] as well as ester[25–27] and amide cleavage[28, 29] followed. The most thoroughly studied model system is that of phosphate hydrolysis, owing to the high impact of phosphate transfer in life processes. Although many phosphate transferring zinc enzymes have di- or trimetallic reaction centers,[4, 30] and bimetallic activation of organophosphates[31–34] and oligophosphates[35, 36] has been demonstrated in zinc complex model studies, it has also been found that one zinc ion is sufficient to effect catalytic phosphate hydrolysis.[1–3, 5, 6] Consequently detailed kinetic and mechanistic studies have been performed on the hydrolysis of

[a] Prof. Dr. H. Vahrenkamp, Dipl.-Chem. M. Rombach, Dipl.-Chem. C. Maurer, Dr. K. Weis
Institut für Anorganische und Analytische Chemie
der Universität Freiburg
Albertstr. 21, D-79104 Freiburg (Germany)
Fax: (+49) 761-2036001
E-mail: vahrenka@uni-freiburg.de

[b] Dr. E. Keller
Kristallographisches Institut der Universität Freiburg
Hebelstr. 25, D-79104 Freiburg (Germany)
Fax: (+49) 761-2036438
E-mail: kell@uni-freiburg.de

Supporting information for this article (tables of zinc–ligand bond distances, bond angles, and of dihedral angles between the faces of the ZnL_5 polyhedra for the 50 [Tp′Zn(X)(Y)] complexes) is available on the WWW under http://www.wiley-vch.de/home/chemistry/ or from the authors.

  0947-6539/99/0503-1013 $ 17.50+.50/0

organophosphates with the aid of $Zn{-}OH_2$ or Zn–OH complexes of polydentate ligands.[37–41] One important consequence of the hydrolysis investigations with enzymes, as well as with model complexes, is that there is good evidence for a concerted or hybrid mechanism involving as the activated zinc-bound species an aggregate like **A,** in which nucleophilic attack of the zinc-bound OH and electrophilic attack of the zinc ion on the substrate occur simultaneously.

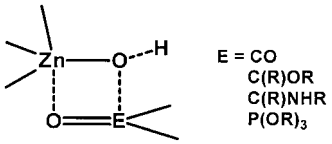

A

This type of four-center intermediate has also been found likely in recently developed theoretical models of CO_2 hydration by carbonic anhydrase.[42, 43]

We have contributed, to this field, the synthesis of the stable pyrazolylborate–zinc hydroxide complexes **1**–**5,**[14, 16, 18, 19] experimental proof that the pK_a values of the corresponding $Zn{-}OH_2$ complexes are at or below 7,[44] and the hydrolytic reactions of these complexes with CO_2,[45, 46] esters and amides,[47] organophosphates,[48] diphosphates,[49] and sugar phosphates including nucleotide derivatives.[50] In a short

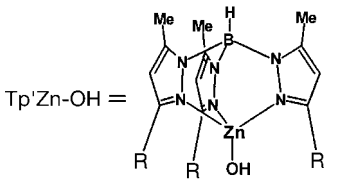

1 $Tp^{t\,Bu,Me}Zn\text{-}OH$: R = (*tert*-butyl)
2 $Tp^{Ph,Me}Zn\text{-}OH$: R = (phenyl)
3 $Tp^{Cum,Me}Zn\text{-}OH$: R = (*p*-cumenyl)
4 $Tp^{Py,Me}Zn\text{-}OH$: R = (pyridyl)
5 $Tp^{Pic,Me}Zn\text{-}OH$: R = (5′-picolyl)

communication Kitajima described similar organophosphate cleavages by another [Tp′Zn–OH] complex.[15] Our work has laid a preparative and structural basis for mechanistic investigations and for a discussion of their potential biological relevance. This paper presents kinetic data for organophosphate and ester cleavages, their interpretation based on an application of the Bürgi–Dunitz structure correlation method, and some generalizations to be drawn thereof for zinc-mediated enzymatic reactions.

Results and Discussion

Organophosphate cleavages

Reaction systems: The [Tp′Zn–OH] complexes **2**, **3**, and **5** were chosen as the hydrolytic agents. They were used to cleave off one aryloxide unit from the triorganophosphates **6a**–**e**: $PO(OPh)_3$ (**6a**), $PO(OPh)_2(ONit)$ (**6b**), $PO(OEt)(ONit)_2$ (**6c**), $PO(Orib)(ONit)_2$ (**6d**), and $PO(ONit)_3$ (**6e**) [Nit = *p*-nitrophenyl, rib = 2,3-isopropylidene-5-methylribosyl]. The reactions proceed according to Equation (1), yielding the zinc diorganophosphate complexes **7**, **8**, and **9**. We have previously described these reactions on a preparative scale and characterized the products.[48–50]

$$\underset{\textbf{2, 3, 5}}{Tp'Zn\text{-}OH} + PO(OR)_2(OR') \rightarrow \underset{\textbf{7a-d, 8b-d, 9b-d}}{Tp'Zn\text{-}OPO(OR)_2} + HOR' \quad (1)$$
$$\textbf{6a-e}$$

Tp′		(OR)$_2$	
7	$Tp^{Ph,Me}$	**a**	$(OPh)_2$
8	$Tp^{Cum,Me}$	**b**	(OEt)(ONit)
9	$Tp^{Pic,Me}$	**c**	(ORib)(ONit)
		d	$(ONit)_2$

We had also observed previously that the phenol HOR′ liberated in these reactions undergoes a condensation reaction with the starting material [Eq. (2)]. This condensation is at least two orders of magnitude faster than the hydrolytic cleavage. It uses up a second equivalent of the starting material [Tp′Zn–OH], which had to be supplied in the reactions on the preparative scale. It posed no problems in the kinetic runs, which were all done with a large excess of [Tp′Zn–OH]. The resulting phenolate complexes **10**–**12** have also been characterized by us before.[48, 51]

$$\underset{\textbf{2, 3, 5}}{Tp'Zn\text{-}OH} + HOR' \rightarrow \underset{\textbf{10, 11, 12}}{Tp'Zn\text{-}OR'} + H_2O \quad (2)$$

Tp′		R′	
10	$Tp^{Ph,Me}$	**a**	**Ph**
11	$Tp^{Cum,Me}$	**b**	Nit
12	$Tp^{Pic,Me}$		

All reactions described here are strictly stoichiometric, that is, they are finished after one turnover. Although they produce one equivalent of water this does not initiate a catalytic cycle, for example, by liberation of the phosphate ligand as the corresponding phosphoric acid and re-formation of the [Tp′Zn–OH] complex. In addition to being unrealistic owing to the acid–base properties of the reagents, this latter process is also unlikely as a result of the high stability of the pyrazolylborate–zinc phosphate complexes. Thus the reaction system described here is limited to the key step of the complex- or enzyme-catalyzed process, namely, the translocation of the zinc-bound OH group to the substrate, concomitant with the liberation of the hydrolysis product HOR′. It should be noted in this context that previous investigations of so-called catalytic zinc complex/organophosphate reaction systems[37, 39–41] also used large excesses of the catalytic zinc compounds and determined k'' values rather than turnover numbers. Our own attempts to make these reactions catalytic have met with little success so far.[52] Although solvent mixtures containing water (e.g., dichloromethane/methanol/water 6:4:1) can be found that will dissolve the complexes [Tp′Zn–OH] and that allow the determination of the pK_a values of the corresponding $Tp'Zn{-}OH_2$ complexes,[53] water could not yet be made a reagent in their chemistry. The advantage of the encapsulation by Tp′ ligands that makes the existence of the Zn–OH function at neutral pH possible is a disadvantage in terms of the formation of

0947-6539/99/0503-1014 $ 17.50+.50/0 *Chem. Eur. J.* **1999**, *5*, No. 3

charged species (i.e., cationic [Tp′ZnL] complexes or intermediates for proton transfers), and also the neutral [TpZn–X] complexes (e.g., phosphates or carboxylates) with their hydrophobic exterior are too stable and too inert as to favor catalytic turnover.

Measurements: The solvent for all kinetic runs was chloroform, its advantage being that it dissolves all reagents and products and does not react with any of them. The starting concentration of phosphates **6b–e** was 0.1 mM. The [Tp′Zn–OH] complexes were added in a 25- to 150-fold excess. The reaction temperatures were 17.5–47.5 °C. The progress of the hydrolyses of **6b–e** was monitored by registering the intensity of the absorption band of the product complexes **10b**, **11b**, or **12b**, which occurs at about 380 nm. Under these conditions the time for completion of the reactions was in the order of 1 hour to 2 days. Measurements were recorded for at least $3t_{1/2}$. For that period all reactions were found to be pseudo-first-order (correlation coefficients >0.999).

Product control by ^{31}P NMR ensured that the cleavages of phosphates **6a**, **6c**, **6d**, and **6e** yielded no other species than those of Equation (1). This means that under the conditions chosen, only one aryloxide unit is cleaved off and this is exclusively *p*-nitrophenolate when it is present. The only exception was the reaction of **2** with phosphate **6b**, which yielded small amounts of [Tp^{Ph,Me}Zn–O–PO(OPh)(ONit)] together with the main product **7a**. However, this did not affect the kinetic results as the byproduct [Tp^{Ph,Me}Zn–OPh] remains unobserved in the range of the visible spectrum measured, and the method chosen for the kinetic analysis eliminates the dependency on the total concentrations of the products.[37] However, in order to avoid complication of the discussion owing to product ambiguities the measurements with phosphate **6b** were limited to this one case.

The kinetics of the cleavage of triphenylphosphate (**6a**) were measured by ^{31}P NMR spectroscopy. Due to the much lower reactivity of **6a**, even high concentrations of phosphate (100 mM) required about 60 hours to reach $3t_{1/2}$. This limited the excess of Tp′Zn–OH and prevented the determination of a precise value of k'' and the activation parameters. The data obtained for the cleavage of **6a** by **2** are nevertheless included in the discussion as a point of reference.

For the reactions monitored by UV/visible spectroscopy, the absorption intensities of **10b**, **11b**, or **12b** were registered continually. They were transformed according to Equation (3) to obtain the pseudo-first-order rate constants k_{obs}. Figure 1 shows the corresponding plots for the cleavage of **6c** by **3** at five different temperatures to demonstrate their linearity up to $3t_{1/2}$.

$$\ln[1-(I_t/I_\infty)] = -k_{obs}t \quad (3)$$

By variation of the excess concentration of the Tp′Zn–OH complexes the second order rate constants k'' were obtained. As an example for this Figure 2 shows the corresponding plots

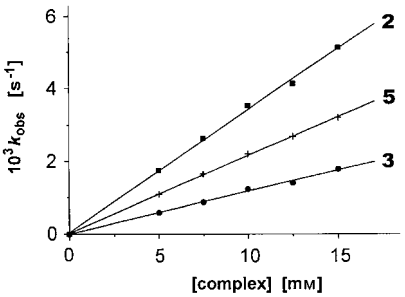

Figure 2. Plots for the determination of k'' from the cleavage of **6d** by **2**, **3**, and **5** at 40 °C.

for the reactions between phosphate **6d** and the three Zn–OH complexes. The correlation coefficients for the least-squares lines through the experimental points are >0.998. The fact that the lines pass through the origin of the coordinate system proves that no other species apart from the [Tp′Zn–OH] complexes are hydrolytically active, as was further verified by the observation of no spectral changes of the reaction solution in the absence of the [Tp′Zn–OH] reagents. In addition the linearity of the graphs in Figure 2 proves that the reactions are cleanly of second order. Together these facts allow the application of Equation (4) for determining the k'' values.

$$k'' = k_{obs}/[\text{Tp′ZnOH}] \quad (4)$$

In order to obtain the activation parameters, the k_{obs} values were determined for a 50-fold excess of Tp′Zn–OH (500-fold excess of [Tp^{Ph,Me}Zn–OH] over **6b**) in the temperature range 17.5° to 47.5 °C. The activation energies E_a were extracted from plots of $\ln k''$ against $1/T$, and the activation enthalpies $\Delta H^{\neq}$ and entropies $\Delta S^{\neq}$ from plots of $\ln(k''/T)$ against $1/T$ in accord with Equations (5) and (6). Figures 3 and 4 show this for the cleavage reactions of phosphates **6c** and **6e**, respectively. The correlation coefficients for the regression lines in these plots were again >0.998.

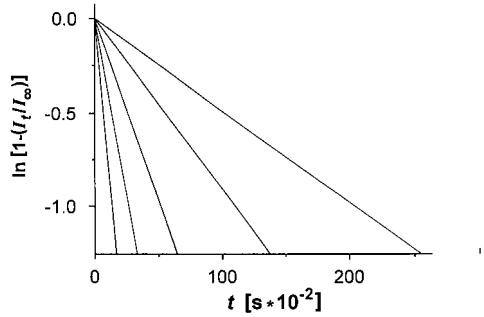

Figure 1. Plots for the determination of k_{obs} from the cleavage of **6c** by **3**. Initial concentration of **6c** = 0.1 mM, of **3** = 5.0 mM. Temperatures 17.5 °C (top line), 25.0, 32.5, 40.0, and 47.5 °C (bottom line).

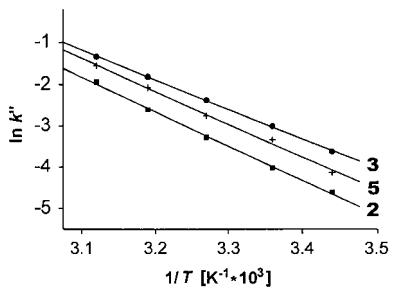

Figure 3. Plot for the determination of E_a from the cleavage of **6c** by **2**, **3**, and **5**.

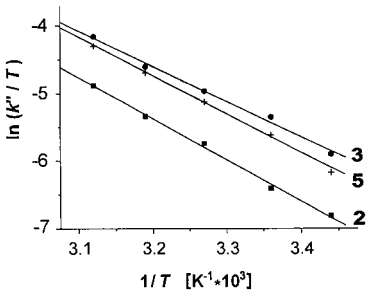

Figure 4. Plot for the determination of $\Delta H^{\neq}$ and $\Delta S^{\neq}$ from the cleavage of **6e** by **2**, **3**, and **5**.

$$k'' = A \exp(-E_a/RT) \quad (5)$$

$$k'' = kT/h \exp(-\Delta H^{\neq}/RT) \exp(\Delta S^{\neq}/R) \quad (6)$$

The influence of solvent polarity was tested for the hydrolysis of phosphate **6d** with all three zinc complexes. Chloroform was replaced by acetonitrile in 10% steps up to a 50:50 composition. The reactions became faster by a factor up to seven. Figure 5 shows this for the case of [Tp^{Pic,Me}Zn–OH] (**5**).

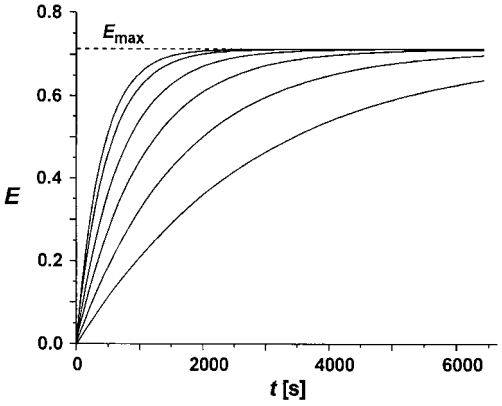

Figure 5. Extinction values measured during the cleavage of **6d** by **5** at 25 °C in $CHCl_3/CH_3CN$ mixtures varying in 10% steps from 50:50 (top line) to 100:0 (bottom line).

Rate constants: All phosphate cleavage reactions are first-order with respect to both the organophosphate and the zinc complex. This implies that both reagents are associated in the rate-determining step. With this observation alone specific statements on the nature of the activated complex are not possible. However, the second-order rate constants (see Table 1) and their variations allow a number of comparisons.

The major influence on the reaction rates rests in the number of *p*-nitrophenolate groups in the organophosphates. One more nitrophenolate causes the reactions to be at least one order of magnitude faster, and tris(*p*-nitrophenyl)phosphate reacts 10^4 times faster than triphenylphosphate. In accord with this, *p*-nitrophenolate is the preferred leaving group, and we have found no cleavage of an alkylphosphate by [Tp′Zn–OH] so far.

Table 1. Second order rate constants k'' [$s^{-1}mol^{-1}$] for the phosphate cleavage reactions at 25 °C.

	[Tp′Zn–OH] reagent		
substrate	**2**	**3**	**5**
6a	0.00016	–	–
6b	0.00082	–	–
6c	0.050	0.018	0.036
6d	0.102	0.034	0.068
6e	1.545	0.452	1.090

The variation of the Tp′ ligands causes a much smaller variation of the reaction rates. On the average the phenyl-substituted system **2** reacts 1.4 times faster than pyridyl-substituted **5** and 3.1 times faster than *p*-isopropylphenyl-substituted **3**. Comparing **2** with **3**, which should be electronically equivalent, the rate difference is explained by the steric hindrance due to the three isopropyl substituents. It seems that the *p*-methyl substituents on the pyridyl rings in **5** also have a retarding influence, which is noticeable yet small, as expected. We had originally expected that the polar pyridyl groups would have an accelerating influence on the polar hydrolysis reactions, but it seems that this influence is outbalanced by the reduction of the Zn–OH nucleophilicity owing to electron withdrawal. This qualitative statement is supported by some rate data on the cleavage of **6d** by the [Tp′Zn–OH] complex **4**, which bears unsubstituted pyridyl rings, indicating that **2** and **4**, which offer identical sterical conditions, produce virtually identical reaction rates.

That the reaction rates respond favorably to more polar conditions is obvious from the influence of solvent polarity. In going from pure chloroform to chloroform/acetonitrile (50:50) the rate for the cleavage of **6d** by **2** rises by a factor of 3.0, for that by **3** by a factor of 3.8, and for that by **5** by a factor of 7.5. Thus the pyridyl-substituted [Tp′Zn–OH] complex shows a much stronger response to a polar influence than the two others. While the overall rate enhancement due to more polar reaction conditions simply reflects the polar nature of the transition state of the hydrolysis, the increased enhancement for **5** seems to indicate that in a polar medium the pyridyl groups can bring their own polarity to effect, for example, by a favorable orientation towards the reacting substrate.

The reaction rates observed here for nonpolar substrates under nonpolar conditions compare favorably with those for the same substrates in solvent mixtures containing water. The alkaline hydrolysis of **6c** under various conditions[39, 54, 55] was found to be 3–7 times faster, and that of **6b**[37] 34 times faster than those observed here for **2**. When zinc complexes of polydentate nitrogen ligands were used, whose hydrolytically active constituent is assumed to be [L_nZn–OH],[37–41, 56] the reaction rates for the hydrolyses in water/organic solvent mixtures were found to be 2–4 times faster than here. All these reactions were investigated in solvents of much higher polarity than ours, and a very high influence of solvent polarity, for example, for the hydrolysis of **6b**,[37, 54] was found for them, as it was found here for the hydrolysis of **6d**. Taking this into consideration it must be concluded that the [Tp′Zn–OH] complexes are indeed powerful nucleophiles. Their hydrolytic activity is surpassed significantly only by that of bifunctional[57] or bimetallic[58] reagents. The reason for their nucleophilic strength must be the fact that the corresponding [Tp′Zn–OH_2]$^+$ complexes have very low pK_a values[44, 53] resulting in the existence of [Tp′Zn–OH] as such under neutral conditions, with their Zn–OH functions being available without assistance by a base.

0947-6539/99/0503-1016 $ 17.50+.50/0 *Chem. Eur. J.* **1999**, *5*, No. 3

Activation parameters: Table 2 lists the activation energies and enthalpies. Their values were obtained for all cleavage reactions investigated here except that of **6a**. The activation energies range from 46 to 69 kJ mol^{-1}. This corresponds roughly to the range found for the alkaline hydrolysis of various organophosphates.[54, 55] To our knowledge activation energies for zinc-complex-mediated organophosphate hydrolyses are not available.

Table 2. Activation energies/enthalpies [kJ mol^{-1}] for the phosphate cleavage reactions.

	[Tp′Zn–OH] reagent		
substrate	**2**	**3**	**5**
6b	55.8/53.3	–	–
6c	58.9/56.4	69.1/66.1	65.9/63.0
6d	57.2/54.7	61.4/58.8	60.7/58.2
6e	45.8/43.3	52.9/50.4	49.7/47.2

Table 3 lists the activation entropies. Typically bimolecular processes have activation entropies around -80 J mol^{-1} K^{-1}.[59] The observed values between -54 and -126 J mol^{-1} K^{-1} fall into this category. Considering that both the reacting Zn–OH and P-OR functions are surrounded by bulky substituents, the observed values must be considered large, that is, there is a high degree of ordering in the transition state. This is our strongest indicator for the intimately associated four-center intermediate as depicted in formula **A**.

Table 3. Activation entropies [J mol^{-1} K^{-1}] for the phosphate cleavage reactions.

	[Tp′Zn–OH] reagent		
substrate	**2**	**3**	**5**
6b	-126	–	–
6c	-80	-54	-62
6d	-80	-76	-75
6e	-98	-81	-86

Again activation entropies for other zinc-complex-mediated organophosphate hydrolyses are not available. Therefore comparisons can only be made between the compounds investigated here. Except for the single value for phosphate **6b**, which is somewhat out of range, the other values show noticeable trends. For each [Tp′Zn–OH] complex phosphate **6c** has the least negative activation entropies, followed by **6d** and then **6e**. For the comparison of **6c** and **6d** this means that the larger molecule of the sugar phosphate **6d** has to give up more of its mobility when approaching the transition state. Comparison **6c** and **6d** with **6e** seems to indicate that the higher polarity of **6e** strengthens the polar interactions in the four-center intermediate and, hence, causes a tighter ordering of its two components. A horizontal comparison in Table 3 shows that for each organophosphate the reagent **2** causes the most negative activation entropy, followed by **5** and then **3**. Considering only the steric bulk of the zinc complexes one would have expected that **3** would induce the highest loss of freedom and, thus, the most negative activation entropies. The observed sequence, however, is inversely related to the steric bulk of the [Tp′Zn–OH] complexes. Thus, if the steric bulk of both reagents is the cause of the ordering of the activation entropies, its effect must be opposite for the phosphates and for the [Tp′Zn–OH] species. For the latter a better approach to the reaction center seems to go along with a higher degree of order in the transition state, and, hence, more negative activation entropies.

Irrespective of their detailed explanations, the strongly negative activation entropies are a new and hitherto unreported piece of evidence for the tightly bound four-center intermediate of organophosphate hydrolysis brought about by zinc complexes or zinc-containing enzymes. Together with the other evidence obtained before, for example, from comparing the reactivity of Zn–OH species with that of free OH^- [37] or from comparing zinc complex reagents with different steric requirements,[39] they leave little doubt that the tightly bound aggregate **A** is the key intermediate in the course of these hydrolytic reactions.

Ester cleavages: Ester cleavages by pyrazolylborate–zinc hydroxide complexes are also strictly stoichiometric [Eq. (7)].[47] They require activated esters like *p*-nitrophenolates or thiophenolates or trifluoroacetates to proceed with a reasonable rate; this limits the choices for kinetic measurements. In the present study it was found that a clean kinetic behavior is observed for esters $CH_3CO–OC_6H_4$-*p*-NO_2 (**13**) and $CH_3CO–SC_6H_4$-*p*-NO_2 (**14**) when treated with pyrazolylborate **3** and leads to the complex [Tp^{Ph,Me}Zn–O–$COCH_3$] (**15**). Just like in the organophosphate cleavages, the liberated phenolate (thiophenolate) uses up a second equivalent of the reagent **3** with formation of [Tp′Zn–OR′] (**10b**) or [Tp′Zn–SR] ([Tp^{Ph,Me}Zn–SC_6H_4-*p*-NO_2]; **16**).

$$[\text{Tp}'\text{Zn–OH}] + \text{RC(O)ER}' \rightarrow [\text{Tp}'\text{Zn-OC(O)R}] + \text{HER}' \ (\text{E} = \text{O, S}) \quad (7)$$

The reactions were followed by the UV/visible spectroscopic technique as described above, that is, the growth of the bands due to **10b** or **16**, respectively, was recorded. The data acquisition, data treatment, and analysis were done the same way as described above for the organophosphates, leading to kinetic parameters of the same quality. Table 4 lists the results for the two cleavage reactions.

Table 4. Kinetic parameters for the cleavage of esters **13** and **14** by complex **3**.

	13	**14**
k''(25 °C) [s^{-1} mol^{-1}]	0.0035	0.0011
E_a [kJ mol^{-1}]	64.3	70.0
$\Delta H^{\neq}$ [kJ mol^{-1}]	61.8	67.5
$\Delta S^{\neq}$ [J mol^{-1} K^{-1}]	-85.6	-76.3

The second-order rate constants, which are in the order of 10^{-3} s^{-1} mol^{-1} at room temperature, are again considerably smaller than those for the hydrolysis of **13** and **14** by aqueous alkali.[60, 61] One would use the same arguments as above to explain this. The activation energies/enthalpies (around 65 kJ mol^{-1}) fall in the same range as observed here for the organophosphates and for alkaline hydrolysis in water,[60, 61] thereby offering no unusual features. The observed activation entropies (around -80 J mol^{-1} K^{-1}) are also of the same size

as those for the organophosphates, and allow us to make the same mechanistic conclusions. It should be noted, though, that activation entropies up to $-100\ J\,mol^{-1}\,K^{-1}$ have been observed for ester hydrolyses,[59b, 61] while those found for the thiol ester **14** here are signifcantly more negative than those reported for alkaline hydrolysis of other thiol esters.[61]

The phenolate **13** is cleaved about three times faster than the thiophenolate **14**. We would have expected a reversed order, considering that thiol esters are much better acylating agents than normal esters. However, as outlined by Janssen[61] the hydrolysis of thiol esters is influenced by more factors than that of normal esters, and both lower and higher relative reaction rates have been observed for it. In terms of the four-center intermediate **A** for the hydrolysis reactions, the slower rate for **14** can be related to the lower basicity of the carbonyl oxygen in thiol esters compared with that in normal esters. Hence, the C=O–Zn interaction and thereby the zinc-induced activation of the carbonyl function may be smaller.

There is ample literature on the metal-complex-mediated hydrolysis of esters,[62] and kinetic data have been reported for several cases where [L_nZn–OH] species are supposed to act as nucleophiles.[26, 27, 31, 39, 63–67] When these species were simple mononuclear zinc complexes, the second-order rate constants for the cleavage of *p*-nitrophenylacetate **13** in water were found in the range 10^{-1} to $10^{-3}\ s^{-1}\,mol^{-1}$. Accelerations by one or two orders of magnitude were observed when the ligands used bore pendant alkoxide groups, which assist the hydrolytic process.[65, 66] Considering that the cleavage of **13** by **3** was performed in chloroform, that is, a solvent of much lower polarity, one can conclude that the hydrolytic activity of **3** actually corresponds to those of the reference compounds, as also evidenced above for the organophosphate cleavages.

Activation energies for zinc-complex-mediated hydrolyses of *p*-nitrophenylacetate were reported only for complexes with [12]aneN$_3$ and [12]aneN$_4$ ligands.[13, 68, 69] They are in the order of 50 kJ mol^{-1}, that is, slightly, though not significantly, smaller than the one observed here. We are not aware of any activation parameters for zinc-complex-mediated hydrolyses of thiol esters nor of any activation entropies for zinc-complex-induced ester hydrolyses.

The overall similarity of the activation parameters for both organophosphate and carboxylic ester cleavages by the [Tp′Zn–OH] complex **3** suggests that the mechanistic scheme for both reaction types is the same. Previously a different mechanistic behavior was proposed for the two reaction types when catalytically active [L_nZn–OH] species were employed.[37, 39] While the so-called hybrid mechanism involving the four-center intermediate **A** was deduced for organophosphates, in the case of esters it was suggested that the [L_nZn–OH] species act as simple nucleophiles. The arguments for the latter rest in the fact that ester cleavage by [L_nZn–OH] is much slower than that by OH^- and that the activities of the various [L_nZn–OH] species are proportional to their basicities. In our case the reaction rates cannot be compared with those for the hydroxide ion in water, since our measurements were made in chloroform. Like the other researchers[37, 39, 65] we do observe that *p*-nitrophenylacetate hydrolysis is 2–3 orders of magnitude slower than tris(*p*-nitrophenyl)phosphate hydrolysis by the same [L_nZn–OH] species. However, in the absence of systematic variations of the substrates or the reaction conditions we have no further arguments for a mechanistic discrimination between organophosphate and carboxylic ester hydrolysis. This makes us emphasize the mechanistic similarity based on the similarity of the activation parameters. We thus propose that the bifunctional-substrate activation with respect to intermediate **A** is operative in both processes. Support for this can be drawn from the aforementioned theoretical studies,[42, 43] which imply the four-center intermediate **A** for the hydrolysis of carbonyl-containing substrates like CO_2. In the following we wish to present structural evidence and geometrical details for this mechanistic proposal.

Proposed reaction trajectory

Geometrical approach: As shown above, there is good evidence for a four-center arrangement (ZnOPO or ZnOCO) in the activated complex of the hydrolysis reactions. This implies that in the course of the reactions the coordination number of zinc increases from four to five and then decreases to four again, the evolution of the coordination pattern being $N_3ZnO^1 \rightarrow N_3Zn(O^1,O^2) \rightarrow N_3ZnO^2$. In the activated complex O^1 and O^2 occupy *cis* positions in the coordination sphere of zinc, and in passing through the transition state the Zn–O^1 bond is given up concomitantly with the formation of the Zn–O^2 bond. There can be little doubt that the entering substrate (represented by O^2) approaches the zinc ion through one N_2O^1 face of the N_3ZnO^1 tetrahedron. Likewise it can be assumed that the completion of the hydrolysis consists in the removal of the nucleophile (represented by O^1) outward from one N_2O^2 face of the resulting N_3ZnO^2 tetrahedron. Both these movements are represented geometrically by a passage along the axis of a distorted trigonal bipyramid. It is important to note that two different N_2O faces, that is, two different trigonal bipyramids, are involved as represented by **B** and **D**.

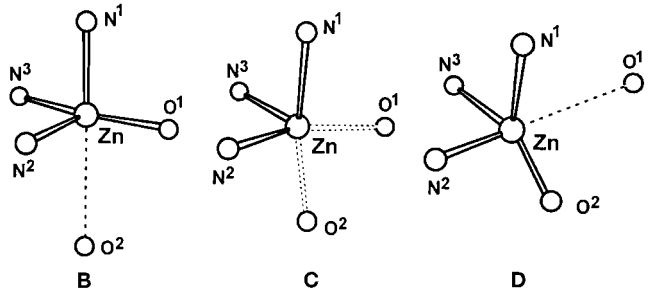

The passage through the transition state then has to be described as a fluxional motion in the ligand sphere of a five-coordinate complex. This sugggests that this motion is the exchange of the axial and equatorial positions of a trigonal bipyramid. Berry pseudorotation has been found to be the lowest-energy pathway for this exchange.[70] Its transition state is a square pyramid. For the hydrolysis reaction this corresponds to **C** with N^3 at the apex, the Zn–O^2 bond half formed, and the Zn–O^1 bond half broken.

Support for this reaction trajectory rests in the structural data of pyrazolylborate–zinc complexes with five-coordinate zinc. While it was originally assumed that pyrazolylborates

0947-6539/99/0503-1018 $ 17.50+.50/0 *Chem. Eur. J.* **1999**, *5*, No. 3

with bulky substituents at the 3 positions are tetrahedral enforcers[71–73] it is now clear that this is not the case. A large number of truly or approximately five-coordinate pyrazolylborate–zinc complexes have been structurally characterized, including examples in which a substrate and a reagent, that is, phosphate and water,[48–50] are coordinated to the same zinc ion. These complexes can be subjected to the structure-correlation method, originally proposed by Bürgi and Dunitz[74] for organic reactions and later applied successfully in coordination chemistry,[75–80] specifically for interconversions of five-coordinate species[74, 78, 79] including S_N2-type ligand substitutions at tetrahedral zinc.[80] The structure-correlation method consists in the suitable superposition of many molecular structures, thereby visualizing a possible reaction pathway. We will show that it is applicable to generate a trajectory for the hydrolytic reactions brought about by [L_3Zn–OH] species.

Data analysis: A search of the documented structure determinations of [Tp′Zn(X)(Y)] complexes, has yielded 52 such coordination environments. A list of them (Table 6) and their computational treatment, is given in the section on structure correlations. They can be grouped into the four classes containing two monodentate (**a**), one chelating bidentate (**b**), or anisobidentate (**c**) ligands, or having Tp′ ligands with one very long (~3 Å) Zn–N interaction and mondentate X and Y ligands (**d**). Of these class **d** is not suitable because it doesn't

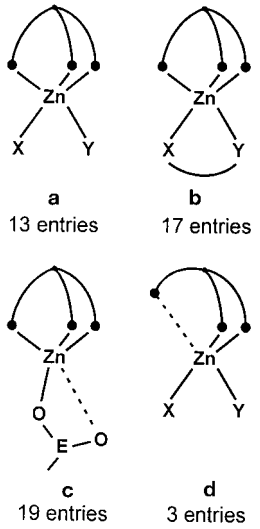

contain truly tridentate Tp′ ligands, and class **c** which is comprised of nitrate, carbonate, and carboxylate complexes doesn't vary enough in terms of deviation from monodentate attachment and from tetrahedral zinc (see below). On the other hand class **b** shows a considerable spread of bond lengths and angles to allow it to be combined with class **a** into the group of truly five-coordinate [Tp′Zn(X)(Y)] complexes, which then has 30 entries.

Various procedures have been described to assess the deviations of five-coordinate species from the ideal trigonal-bipyramidal (TBP) or square-pyramidal (SP) geometries.[74, 78–83] As a rule they have found that the deviations follow the Berry transition, that is, the observed geometries lie on the lowest energy pathway from the trigonal bipyramid to the square pyramid. The simplest method to visualize this uses the two largest bonding angles of the AB_5 species.[82, 83] Referring to the numbering scheme given in the inset of Figure 6, we will address these two angles as $\alpha1$ (1–5) and $\alpha2$ (2–4). $\alpha1$ and $\alpha2$ adopt the values 180°/120° for the TBP case

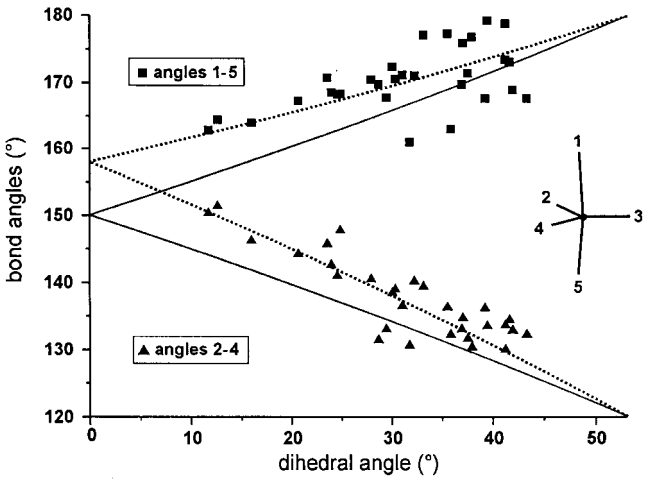

Figure 6. Plot of the two largest bond angles $\alpha1$ (1–5) and $\alpha2$ (2–4) against the dihedral angle δ_{24} (the angle between the normals to the two triangular faces 1–2–4 and 5–2–4) for the 30 complexes of groups **a** and **b**. For the ideal SP δ_{24} is 0°, for the ideal TBP 53.1°.

and 150°/150° for the SP case. As $\alpha1_{TBP} - \alpha1_{SP} = \alpha2_{SP} - \alpha2_{TBP}$ we can assume that during the TBP→SP transition the 180° angle of the TBP shrinks steadily by the same amount that the 120° angle grows until both have reached 150°. A plot of these two angles against a suitable coordinate should be a graphical representation of the Berry transition. Exellent agreement was found for pentacoordinated phosphorus compounds when the dihedral angle δ_{24} between the two triangular faces joined by the vertices of $\alpha1$ and $\alpha2$ is used as this coordinate.[82] A plot of this kind is given in Figure 6 for the 30 selected [Tp′Zn(X)(Y)] complexes.

The two curves describing the Berry transition for ideal complexes (with ideal corresponding to uniform bond lengths and symmetry C_{2v}) are given as solid lines. The two Berry lines have been calculated under the above assumption, that is, with $\alpha1 = 180° - \varepsilon$ and $\alpha2 = 120° + \varepsilon$ ($\varepsilon = 0$ to 30°). It should be noted that these two Berry lines are only approximately straight. For ideal complexes, the dihedral angle δ_{24} is a nonlinear function of $\alpha1$ and $\alpha2$ according to Equation (8) (see section on structure correlations for details).

$$\tan(\delta_{24}/2) = (\cos(\alpha2/2) - \cos(\alpha1/2))/\sin(\alpha1/2) \quad (8)$$

In principle, our data in Figure 6 show the characteristic fork-like distribution described by the two Berry lines. The fit is only poor, however. A much better fit is obtained for a modified model of the Berry pseudorotation, which uses an ideal SP with basal *trans* angles of 158° instead of 150°. The theoretical curves calculated for this case are given as dotted lines in Figure 6. The significantly improved fit makes it imperative to base our model on this modified SP, which is in

excellent agreement with the observations by Dunitz and Bürgi, who found that for pentacoordinated metal complexes the SP arrangement typically has basal angles around 160°.[74] Thus it can be concluded that the 30 zinc complexes considered here have structures close to the Berry transition. It is also obvious from Figure 6 that neither the ideal SP nor the ideal TBP geometries are reached by these zinc complexes.

In order to quantify the latter statement a different approach is appropriate that was first applied by Muetterties.[81] It is based on summing up the values of $\Delta\delta$ for all edges of the AB_5 polyhedra, with δ being the dihedral angles for each edge of the polyhedra and Δ being the absolute difference between a δ_{obs} and the corresponding δ_{ideal} for an SP or a TBP, respectively.[82] Thus for an ideal TBP the sum of $\Delta\delta_{TBP}$ is zero and the sum of $\Delta\delta_{SP}$ is 217.7° (SP with basal *trans* angles of 150°), and vice versa for SP. In a plot of $\Sigma(\Delta\delta_{TBP})$ versus $\Sigma(\Delta\delta_{SP})$ a straight line connecting the 217.7° positions on both coordinate axes represents the Berry path, and it was found that structures of phosphoranes[82] or simple ZnL_5 complexes[80] adhere closely to this straight line.

In a plot of this type (see Figure 7) the Tp′Zn complexes are clearly located in two different regions. While the truly five-coordinate complexes of classes **a** and **b** are positioned on or near the Berry line, those of class **c** form a cluster severely displaced from it. This observation is the basis of the above-made statement that the class **c** complexes do not vary enough in their structures and are not suitable for the following discussion. The 30 class **a** and **b** complexes are, however, positioned close enough to the Berry line to be identified as representing a Berry-pseudorotation-like transition of their structures from the TBP to the SP geometries.[84]

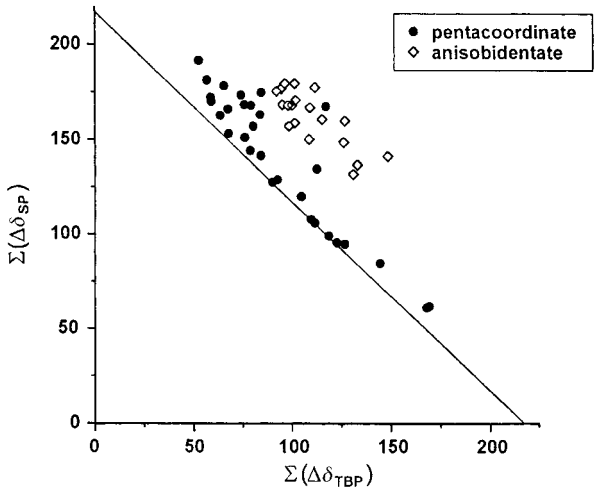

Figure 7. Plot of dihedral angle differences for the zinc complexes of classes **a** and **b** (filled circles) and of class **c** (open diamonds). The straight line corresponds to the ideal TBP →SP transition. For the definiton of $\Delta\delta$ see text.

Adaptation and visualization: While in Figure 7 the fit of the points for the class **a** and **b** complexes to the Berry line is better than for the class **c** complexes, it isn't excellent either. This can be explained by the fact that the coordination geometries of our complexes differ systematically from the geometries of simple AB_5 species. For once, this is due to the limited flexibility of the tridentate Tp′ ligands (whose donor atoms N1, N2, N3 occupy the positions 1, 2, and 3 in Figure 6) which favor intraligand valence angles close to 90°. The complexes can therefore neither adopt the ideal TBP geometry with one angle of 120° nor the ideal SP geometry with two angles of 105° between N1, N2, and N3. Furthermore the SP geometry with which our complexes have to be compared has turned out to be one with basal *trans* angles of 158° instead of 150° (see above). Therefore it seemed appropriate to us to adjust the two prototypes, ideal TBP and SP, due to these restraints. This was done in a procedure that is outlined in the section on structure correlations, by use of the basal *trans* angles of 158° for SP and adhering to no other boundary conditions than those imposed by the Tp′ ligands. The resulting adapted TBP (TBP′) has an axial angle of about 170°, and angles of about 130°, 130°, and 100° in its equatorial plane. The adapted SP (SP′) has two basal angles of 158° and two apical angles each of 93° and 108°. Both adapted geometries were confined to have C_m symmetry. The summing up of their dihedral angle differences leads to a value of $\Delta\delta =$ 202.3° as compared to 217.7° for the ideal TBP and SP.

Based on the adapted TBP′ and SP′ geometries a new correlation diagram can be computed; this is displayed in Figure 8. By applying the $\Delta\delta$ procedure as above to all 30 complexes of class **a** and **b**, with the dihedral angles of TBP′ and SP′ as reference values, the points in Figure 8 result. Their adherence to the adapted Berry line is striking and gives justification to the applied procedure. While again the extremes of the pure adapted TBP′ or SP′ are not reached, the adapted Berry transition is clearly identified as the pathway of the structural interconversion.

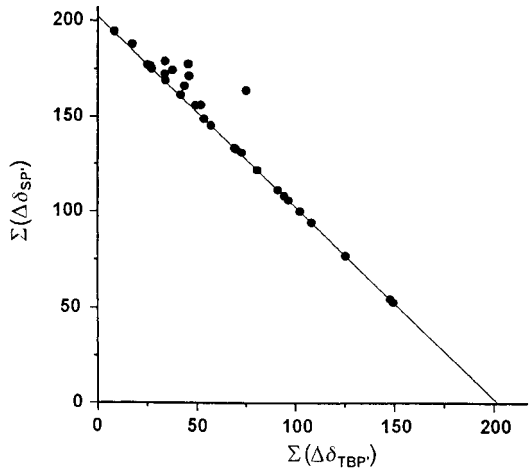

Figure 8. Plot of dihedral angle differences for the 30 zinc complexes of classes **a** and **b**. The straight line corresponds to the transition between the adapted TBP′ and SP′. For definitions see text.

Figures 7 and 8 and their $\Sigma(\Delta\delta)$ values yield directly a measure for the amounts with which any one of the two prototype structures are realized for a certain complex. Thus, for Figure 7, $(217.7 - \Sigma(\Delta\delta_{SP})/217.7$ gives (amount SP) in the range 0 to 1, while $(217.7 - \Sigma(\Delta\delta_{TBP})/217.7$ gives (amount TBP) in the range 0 to 1. For points on the Berry line, (amount

0947-6539/99/0503-1020 $ 17.50+.50/0 *Chem. Eur. J.* **1999**, *5*, No. 3

TBP) + (amount SP) = 1, that is, (amount TBP) = [1 − (amount SP)]. For points above the line, (amount TBP) is not equal to [1 − (amount SP)], and an averaged value for (amount TBP) can be calculated from Equation (9).

$$(\text{amount TBP})^{av} = \{(\text{amount TBP}) + [1 - (\text{amount SP})]\}/2 \quad (9)$$

These considerations also pertain to the parameters (amount SP′) and (amount TBP′), which can be obtained from the values visualized in Figure 8, and quantitatively as described above, but with the $\Delta\delta$ sum of 217.7° replaced by 202.3°.[85]

The values of (amount TBP)^{av} thus obtained for the 30 class **a** and **b** complexes range from 0.24 to 0.83. This quantifies the statement made above that they reach neither the ideal TBP nor the ideal SP geometries. In comparison the values of (amount TBP′)^{av} range from 0.27 to 0.96. Thus the adapted TBP′ is realized to a rather good approximation by some of the complexes, as is also visible in Figure 8.

The geometrical constructions displayed in Figures 6–8 do not visualize the actual motions in space accompanying the structural changes between the 30 complexes of classes **a** and **b**. This is done in Figure 9,[85] which is meant to display their adherence to the Berry pathway, specifically its adapted version TBP′ →SP′ (see above). In Figure 9 (and in Figures 11 and 12) the pyrazolylborate–zinc unit is reduced to the BN_6Zn bicyclooctane skeleton, atoms N1, N2, N3 correspond to positions 1, 2, and 3 in the inset of Figure 6, and atoms X4 and X5 correspond to positions 4 and 5. The ZnL_5 units in Figure 9 are in approximately the same orientation as the inset in Figure 6, emphasizing the trigonal bipyramidal view of the complexes.

In order to construct Figure 9 a unified labelling scheme had to be applied to all 30 complexes [Tp′Zn(X)(Y)]. Of the ligands X and Y, the one with the longest Zn–L bond was defined to be Y, and its atom bonded to Zn was assigned label Y5 (cf. label 5 in Figure 6). The atom transoid to it, that is, the one defining the largest bond angle, was assigned label N1 (cf. label 1 in Figure 6). Then, as a rule, the second largest bond angle was used to assign label N2, roughly transoid to X4. This leaves an unambiguous assignment of label N3, which in the course of the TBP′ →SP′ transition becomes the apical atom of the square pyramid. This labeling scheme ensures comparability of all complexes and confines the spatial changes covered by all 30 complexes in Figure 9 to one TBP′ →SP′ transition, that is, half the Berry pseudorotation.

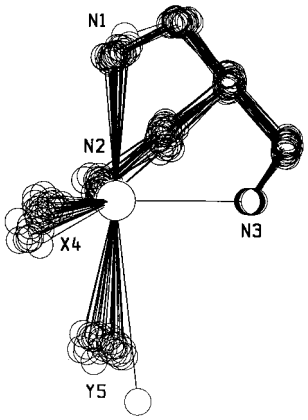

Figure 9. Superposition of the structures of the 30 class **a** and **b** complexes with Zn, N1, and N3 in the plane of projection and Zn–N3 horizontal. For definitions see text.

In order to compare the real motion in space displayed in Figure 9 with the theoretical path of the TBP′ →SP′ transition, Figure 10 was constructed in accordance with the definition given above for the adapted TBP′ and SP′. In Figure 10 three ZnL_5 units are portrayed, corresponding to the starting TBP, that is, TBP′^{1} (solid lines), the transition state SP′ (dashed lines) and the final TBP (see below; i.e., TBP′^{2}; dotted lines). The transition displayed in Figure 9 corresponds to the transition from the solid-line figure to the dashed-line figure in Figure 10. It can be seen that the ranges in space covered by the 30 structures in Figure 9 and by the TBP′^{1} →SP′ transition in Figure 10 are the same.

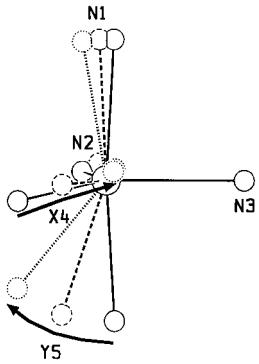

Figure 10. Superposition of the ZnL_5 polyhedra for the adapted geometries TBP′^{1} (solid lines), SP′ (dashed lines), and TBP′^{2} (dotted lines). For definitions see text. Orientation as in Figure 9.

The orientation of the structures in Figure 9 is such that N1 and (less strictly) Y5 are supposed to move in the plane of the drawing, while N2 and X4 are supposed to move roughly in a plane perpendicular to it, as they do to a good approximation. During the simultaneous motion of X4 and Y5, the Zn–Y5 bond gets shorter from right to left, as is visible, while the Zn–X4 bond gets longer from back to front, accompanied by the narrowing of the N1-Zn-Y5 (1–5) and the widening of the N2-Zn-X4 (2–4) bond angles. Specifically, among the 30 complexes of classes **a** and **b**, the N1-Zn-Y5 angle has a minimum value of 159° (theoretical minimum 158°), the N2-Zn-X4 angle has a maximum value of 151° (theoretical maximum again 158°). With respect to the bond lengths, Zn–Y5 varies between 3.02 and 2.04 Å, Zn–X4 between 1.85 and 2.03 Å [excluding bonds to sulfur (max. 2.35 Å) and iodine (2.51 Å)], Zn–N1 varies between 2.49 and 2.07 Å, Zn–N2 between 2.01 and 2.12 Å, and Zn–N3 also between 2.01 and 2.12 Å. Thus the actual motion of the structures in space verifies the results of the computational approach underlying Figures 6–8 and confirms again that this motion is a Berry pseudorotation.

Proposed trajectory: Figure 9 displays one half of the TBP′^{1} →SP′ →TBP′^{2} transition. During the passage from TBP′ to SP′ the axial bonds Zn–Y5 shrink by roughly 1 Å, and simultaneously the equatorial bonds lengthen by about 0.2 Å (excluding Zn–S and Zn–I); the shortest Zn–Y5 bond (2.04 Å) is virtually identical to the longest Zn–X4 bond (2.03 Å), though not in the same molecule. Now, if the transition TBP′^{1} →SP′ is contained in the set of the 30 structures, the same must be valid for the transition TBP′^{2} →SP′ (or SP′ →TBP′^{2}) as TBP′^{1} and TBP′^{2} should have identical (or very similar) structures and both transitions share the same SP′. The 30 structures are therefore suitable to visualize this second transition as well. To have both transitions displayed in

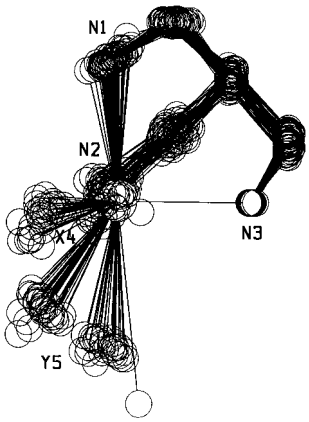

Figure 11. Reaction trajectory built by superposition of two views of the structures of the 30 class **a** and **b** complexes. For definitions see text. Orientation as in Figure 9.

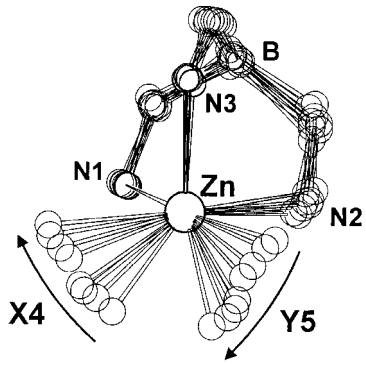

Figure 12. Reaction trajectory built by superposition of four selected structures (see text and Figure 11). The drawings were constructed by placing Zn and N3 in the projection plane and fixing the orientation of the Zn–N1 bond to the back left.

one and the same picture, the ligands named Y during the first transition (i.e., those ones that are axial with respect to TBP′1) must play the roles of X for the second transition (i.e., become equatorial with respect to TBP′2) and vice versa. Practically this means that for the visualization of the second transition the atoms N1 of all the 30 complexes have to be renamed N2 (thus implying X4 to become Y5, see above) and the atoms N2 have to be renamed N1 (which automatically converts the old Y5 into X4). Since interchanging N1 and N2 is equivalent to a mirror operation, the 30 structural drawings also had to be mirrored before plotting and then aligned the same way as the original set. The 60 molecular structures superimposed this way are displayed in Figure 11, showing the same orientation of the pyrazolylborate-zinc unit as applied in Figure 9.

In Figure 11 ligand atom Y5 moves roughly in the plane of the projection again, and ligand atom X4 moves towards the viewer, that is, roughly perpendicular to it. There is a gap between the two groups of 30 structures each, corresponding to the above-mentioned fact that the real transition state, that is, the true square-pyramidal coordination of zinc (SP *or* SP′), is not fully realized, the maximum (amount SP) or (amount SP′) being around 75 %. The total angular motion of Y5 (and likewise X4) is roughly 50°. The total bond shortening of Zn–Y5 (and vice versa the bond lengthening of Zn–X4) is from 3.02 Å to 1.85 Å. The total motion in space converts TBP′1 with N1 and Y5 on the axial positions to TBP′2 with N2 and X4 as axial ligands. Figure 11 can again be compared with Figure 10, now including the dotted-line figure corresponding to TBP′2. As expected, the motion in space in Figure 11 is about twice as large as that in Figure 9 both for X4 and Y5. It is important to note that the tridentate Tp′ ligand adjusts to the motions of X4 and Y5, that is, when Zn–Y5 is long so is Zn–N1 and vice versa. The total bond-length range thus covered by Zn–N1 (and its mirrored counterpart Zn–N2) is from 2.49 to 2.01 Å. As required by the symmetry conditions of the Berry pseudorotation the Zn–N3 bond, which in principle does not move, shows a bond length spread of just 0.1 Å. For this reason it was also chosen to fix the orientation of the Zn–N3 bond when constructing Figures 9–11.

In order to generate a less crowded view of the proposed reaction trajectory, four complexes [Tp′Zn(X)(Y)] were selected that represent approximately equidistant steps along this trajectory. They are [$Tp^{Cum,Me}$Zn(2-hydroxamato-4-methylpentaoylalanylglycylamide)],[87] one half of [$(Tp^{Py,Me}Zn)_2O_2H_3$]ClO_4,[44] [$Tp^{Pic,Me}$Zn-(nitrophenylribosylphosphate)]·H_2O,[50] and [$Tp^{Cum,Me}$Zn(acetohydroxamate)].[87] Their values of (amount TBP′)^{av} are 0.88, 0.73, 0.47, and 0.26, respectively. As described before for Figure 11 they were projected twice, yielding a total of 8 reaction steps. Figure 12 displays the reaction coordinate thus generated, emphasizing the significant distances covered by the motions of X4 and Y5, which are the equivalents of O1 and O2 in formulas **B**, **C**, and **D**.

Altogether the accumulated evidence justifies the statement that the structure correlation method is applicable here. It has yielded a reaction trajectory for zinc-mediated hydrolyses that lets the substrate approach the zinc ion along the axis of a trigonal bipyramid and lets the former zinc-bound OH function leave along the axis of another trigonal bipyramid. The essential feature of the reaction mechanism, that is, the four-center ZnOPO or ZnOCO intermediate, is composed and decomposed in a molecular motion along the Berry pathway. The multitude of structures discussed here, in accord with molecular mechanics calculations,[70] demonstrates that this is a low-energy process with the square pyramidal arrangement as an easily accessible transition state. Recent theoretical treatments of Zn–OH effected hydrolyses in enzymes, specifically CO_2 hydration in carbonic anhydrase,[42, 43] have detailed the 4 → 5 → 4 sequence of coordination numbers at zinc, and the formation and opening of the four-center intermediates. Our work adds experimental evidence and geometrical details to this, resulting from the multitude of static situations in small molecular complexes.

The proposed reaction trajectory, just like the kinetic studies outlined above, describes the reaction pathway for an interconversion starting from a stable reactant [L_3Zn–OH] and ending with a stable product (L_3Zn-phosphate or L_3Zn-carboxylate). This has the advantage of yielding detailed information and the disadvantage of being incomplete in terms of a catalytic process. The latter requires ligand substitution in the product complex by a water molecule and its subsequent deprotonation. It is likely, though not implied by the present study, that the ligand substitution follows a similar course as the hydrolysis, that is, it is a S_N2-type process with X entering and Y leaving on the same side of the zinc ion. Likewise the present study gives no

0947-6539/99/0503-1022 $ 17.50+.50/0 *Chem. Eur. J.* **1999**, *5*, No. 3

information related to the atomic motions in the substrates (phosphates, esters, etc.). Our results are, however, compatible with the standard mechanisms developed for nucleophilic substitutions at phosphates[88] or acyl compounds,[60, 89] which involve pseudorotation at five-coordinate phosphorus or facial attack at sp^2 configured carbon. One might have expected that the structures of class **c** (carboxylate and nitrate) complexes would yield this type of information, but as shown above they are all too similar as to be subjected to a structure correlation analysis. On the other hand, among the complexes of class **b** there are several with five-membered and two with four-membered chelate rings that all fit well on the proposed reaction trajectory, thereby proving that the intimate association of the four atoms in the four-center intermediate near the SP transition state is compatible with the geometrical constraints of the substrates as well.

The present work has produced experimental data for the hydrolysis of organophosphates and carboxylic acid esters. The [Tp′Zn−OH] complexes have also been found to hydrolyze pyrophosphates,[49] amides,[47] and CO_2.[45, 46] The mechanistic details of pyrophosphate cleavage should correspond to those of organophosphate cleavage, and the details of amide, peptide, and CO_2 hydrolysis to those of ester hydrolysis. Viewed from the Tp′Zn unit the atomic motions during the reactions are equivalent in all cases. The conclusions drawn here from the kinetic data and the structure correlations should therefore apply equally well to the other hydrolytic reactions. Accordingly we propose that the reaction trajectory developed here is valid for all hydrolytically active [L_3Zn−X] species and for all hydrolyzable substrates.

The final question to be addressed is that whether the reaction system described here is a suitable model for the hydrolytic processes occurring in zinc enzymes. We think that this is the case within the limitations chosen. The pyrazolylborate ligands create a hydrophobic pocket around the metal ion, and they are flexible to a certain, yet not unlimited, degree. Just like the enzymatic environment that holds the zinc ion in place by three side-chain donor functions the Tp′ ligands allow access of the substrate to the functional [L_3Zn−OH] unit, and they accommodate the coordination number changes of the metal as well as the $TBP^1 \rightarrow SP \rightarrow TBP^2$ interconversions. The pyrazolylborate–zinc complexes do not yield catalytic reactions due to their hydrophobic nature and the high stability of the product complexes. Furthermore, they cannot reproduce details of the enzymatic situation like secondary interactions, polar substrate channels, or proton transfer pathways. However, in return they have given easy access to thermodynamic and mechanistic details of an essential part of the catalytic cycle, the concerted hydrolytic process in the coordination sphere of zinc.

Conclusions

The combination of kinetic data and structural comparisons has delivered a consistent picture of the hydrolysis of esters of phosphoric and carboxylic acids by pyrazolylborate–zinc hydroxide complexes. The essential observations are the strongly negative activation entropies of the reactions and a systematic structural correlation between 30 complexes of the type [Tp′Zn(X)(Y)]. The essential features deduced are i) double activation of the substrates by means of coordination of a substrate oxygen to zinc with simultaneous attack of the zinc-bound hydroxide at the substrate and ii) a reaction pathway involving Berry pseudorotation at five-coordinate zinc during the trajectory, beginning with the approach of the substrate and ending with the release of the products. Although the investigated hydrolysis reactions are stoichiometric, their course can be used to describe related catalytic reactions. Likewise the geometrical restraints of the pyrazolylborate ligands can be taken as analogous to those of a protein environment in a zinc enzyme. It is therefore proposed that the atomic motions in the ligand sphere of zinc may proceed in a similar fashion in hydrolytic zinc enzymes.

Experimental section

Materials: The [Tp′Zn−OH] complexes[16, 18, 19] were prepared according to the published procedures. Esters and organophosphates were obtained commercially or prepared as cited in ref.[48–50] Solvents were obtained commercially and used as supplied.

Kinetic measurements by UV/visible spectroscopy: These measurements were carried out in chloroform with a Jasco V-570 spectrophotometer. The temperature in the UV cell was held constant at 17.5, 25.0, 32.5, 40.0 and 47.5 °C for **6b–e**, and at 15.0, 20.0, 25.0, 30.0 and 35.0 °C for **13** and **14**. For the reactions the change in the absorption intensities at either 371 or 418 nm, resulting from the formation of **10b** (λ_{max} = 375.3 nm), **11b** (λ_{max} = 378.1 nm), **12b** (λ_{max} = 365.8 nm), and **16** (λ_{max} = 419.4 nm) was recorded automatically every 10 s. The increase in absorption intensities was recorded until the hydrolysis was 90% complete. The end points were determined after $t > 5t_{1/2}$. All hydrolysis reactions showed excellent first-order behavior up to $3t_{1/2}$ for **6b–e**, **13**, and **14**, with correlation coefficients better than 0.998. The pseudo-first-order rate constants were obtained by a ln-plot method. From the slope of k_{obs} against the concentration of the [Tp′ZnOH] complexes the second-order rate constants were obtained. After verification of the rate law, k'' was obtained directly using Equation (4). This was justified by the linearity of plots of k_{obs} versus [Tp′ZnOH] and their y intercepts at [Tp′ZnOH] = 0. The reproducibility of the obtained rate constants was checked regularly. The error was within 5%.

*Hydrolysis of **6b–e***: Stock solutions of various concentrations of **2**, **3**, and **5** were prepared. These stock solutions (1.9 mL) were allowed to equilibrate in the UV cell. The phosphate ester stock solutions were allowed to equilibrate in a separate flask. After 30 min these ester stock solutions (0.1 mL) were added to the UV cell. For the hydrolysis of **6c–e** the starting concentrations in the cell were 0.1 mM of the phosphate esters and 2.5, 5.0, 7.5, 10.0, and 12.5, and 15.0 mM of the [Tp′ZnOH] complexes **2**, **3**, and **5**. For the hydrolysis of **6b** they were 0.1 mM of the phosphate ester and 20, 30, 40, 50, and 60 mM of **2**. The rate laws were determined for the reaction of the zinc complexes **2**, **3**, and **5** with the phosphate esters **6c** and **6e** at 25 °C and with **6b** and **6d** at 40 °C. The other k'' values at different temperatures were obtained directly with 5 mM solutions of **2**, **3**, and **5** for the cleavage of **6c–e**, and with 50 mM solutions for the cleavage of **6b**, using Equation (4).

*Hydrolysis of **13** and **14***: Stock solutions of various concentrations of **2, 13**, and **14** were prepared. They were allowed to equilibrate in UV cells. After 30 min both **2** and **13** or **14** stock solutions (1 mL each) were mixed in the UV cell. The starting concentrations in the cell were 0.25 mM of the ester and 22.5, 30.0, 37.5, 45.0, 52.5 and 60 mM of **2**. The subsequent procedure was as described above.

Kinetic measurements by NMR spectroscopy: For these measurements a Varian U-300 spectrometer was used. The solvent was deuterated chloroform. The temperature in the NMR tubes was held constant at 27.0 °C. Spectra were recorded at intervals between 25 and 720 s. The reactions were followed until the hydrolysis was 90% complete. The intensities of the ^{31}P NMR signals of **6a** and **7a** were used to obtain the kinetic data. They were found to be reproducible to within 10%.

Hydrolysis of ***6a***: Compounds **2** (56.6 mg, 0.10 mmol) and **6a** (17.8 mg, 0.057 mmol), and $CDCl_3$ (600 μL) were mixed in a NMR tube, yielding a concentration of 167 mM of **2** and 95.0 mM of **6b**. At 27 °C the ^{31}P NMR signals at $\delta = -16.63$ for **6b** and at $\delta = -17.78$ for **7a** were recorded every 12 min for 60 h. For an estimation of k'' the formula $k''t = K$ with $K = \{1/([A]_0 - 2[B]_0)\} \ln\{([B]_0([A]_0 - 2[D]_t))/(([B]_0 - [D]_t)[A]_0)\}$ was used, which is based on a second order reaction $A + 2B \rightarrow P$(P = products = C + D, D = **7a**) with the rate law $v = k''[A][B]$.[90] k'' was then obtained from a plot of K against t. The correlation coefficient up to 70% reaction completion was better than 0.998.

Table 5. Subsituents R^1 and R^2 in the Tp ligands.

ligand	R^1	R^2
Tp^{tBu}	*tert*-butyl	–
$Tp^{tBu,Me}$	*tert*-butyl	methyl
Tp^{Ph}	phenyl	–
$Tp^{Ph,Me}$	phenyl	methyl
$Tp^{iPr,iPr}$	*iso*-propyl	*iso*-propyl
$Tp^{Cum,Me}$	cumenyl (*p*-isopropylphenyl)	methyl
$Tp^{Py,Me}$	3-pyridyl	methyl
$Tp^{Pic,Me}$	picolyl [3-(5-methyl)-pyridyl]	methyl

Structure Correlations

Terminology of complexes [Tp′Zn(X)(Y)]: The symbol Tp is used for hydrotris(pyrazolyl)borato ligands. The symbol Tp′ is used as a general abbreviation for substituted Tp ligands. The symbols $Tp^{R1,R2}$ are used for Tp ligands with substituents R1 in position 3 and substituents R2 in position 5 of the pyrazole rings, as outlined in Table 5. Table 6 displays the list of [Tp′Zn(X)(Y)] complexes, classes **a**–**d**. The bond lengths and angles involving zinc as well as all dihedral angles for the coordination polyhedra are tabulated in the Supporting Information for all 52 complexes (Tables S1–S3).

Geometrical treatment

General: For all 52 complexes a unified labelling scheme for the ZnL_5 unit and a unified approach to the analysis of bonding and dihedral angles were applied. For the $[Tp'ZnL_2]$ system the ligand with the longer Zn–L bond was labelled Y, the other X. The corresponding ligand atoms coordinated to Zn were labelled Y5 or 5 and X4 or 4. Of the three Tp′ nitrogen donor atoms the one trans to Y was labelled N1 or 1, the one which in general defines the second largest bonding angle (i.e. the one transoid to X) was labelled N2 or 2. Thus N1(1) and Y5(5) define the axis of a trigonal bipyramid, while N1(1), N2(2), X4(4) and Y5(5) define the base of a square pyramid. The remaining N donor atom (as a rule the one with the shortest Zn–N bond) was labelled N3(3). Throughout the main text the atomic labelling (N1, N2, ..) is applied. In the tables given here and in the Supporting Information we use the numeric labelling (1, 2 ..). For the geometrical analysis, that is, the computation of dihedral angles, the coordination polyhedra were based on the bonding angles at zinc (i.e., all bond lengths were reduced to unity). For most complexes in classes **a** and **b** this yielded results very similar to those obtained by use of the real bond lengths. However, for classes **c** and **d** containing the complexes with one very long Zn–L interaction, the treatment using the real bond lengths produced unrealistic descriptions of

Table 6. Listing of complexes [Tp′Zn(X)(Y)].

	complex	ref.
class a	([Tp′Zn(X)(Y)] with monodentate X and Y)	
1	$Tp^{Pic,Me}$Zn-bis(nitrophenyl)phosphate · H_2O	[48]
2	$Tp^{Pic,Me}$Zn-diphenylphosphate · H_2O	[49]
3	$Tp^{Pic,Me}$Zn-(ribosyl)(*p*-nitrophenyl)phosphate · H_2O, molecule 1	[50]
4	$Tp^{Pic,Me}$Zn-(ribosyl)(*p*-nitrophenyl)phosphate · H_2O, molecule 2	[50]
5	$Tp^{Cum,Me}$Zn-methylsulfonate · H_2O	[91]
6	$[(Tp^{Py,Me}Zn)_2H_3O_2]ClO_4$, unit 1	[44]
7	$[(Tp^{Py,Me}Zn)_2H_3O_2]ClO_4$, unit 2	[44]
8	$[(Tp^{Pic,Me}Zn)_2H_3O_2]ClO_4$, unit 1	[44]
9	$[(Tp^{Pic,Me}Zn)_2H_3O_2]ClO_4$, unit 2	[44]
10	$[(Tp^{Py,Me}Zn\text{-}F)_2]$	[19]
11	$[(Tp^{Py,Me}Zn\text{-}I)_2]$	[19]
12	$[(Tp^{Py,Me}Zn$-*p*-nitrophenolate$)_2]$	[92]
13	$[\{\{Tp^{Py,Me}$Zn-bis(nitrophenyl)phosphate$\}_2Zn(H_2O)_2$(bis-*p*-nitrophenylphosphate$)_2]]$	[48]
class b	([Tp′Zn(X)(Y)] with X and Y part of a chelate ligand)	
14	$Tp^{Cum,Me}$Zn-cumoylacetonate	[87]
15	$Tp^{Cum,Me}$Zn-2-formylphenolate	[93]
16	Tp^{Ph}Zn-acetylacetonate	[94]
17	$Tp^{Cum,Me}$Zn-S-cysteinate, molecule 1	[18]
18	$Tp^{Cum,Me}$Zn-S-cysteinate, molecule 2	[18]
19	$Tp^{Cum,Me}$Zn-ZINCOV (peptide-hydroxamate), molecule 1	[87]
20	$Tp^{Cum,Me}$Zn-ZINCOV (peptide-hydroxamate), molecule 2	[87]
21	$Tp^{Cum,Me}$Zn-acetohydroxamate, molecule 1	[87]
22	$Tp^{Cum,Me}$Zn-acetohydroxamate, molecule 2	[87]
23	$Tp^{Cum,Me}$Zn-acetazolamide	[95]
24	$Tp^{Cum,Me}$Zn-di-*tert*-butylcatecholate, molecule 1	[96]
25	$Tp^{Cum,Me}$Zn-di-*tert*-butylcatecholate, molecule 2	[96]
26	$Tp^{Cum,Me}$Zn-phthalimidocatecholate	[97]
27	$Tp^{Cum,Me}$Zn-phthalimidocatecholate radical anion	[97]
28	$(Tp^{Cum,Me}Zn)_4$(Ni-phthalocyanine-catecholate)	[97]
29	$Tp^{Cum,Me}$Zn-thiouracilate	[98]
30	$(Tp^{iPr,iPr}Zn)_2$-μ-carbonate, Zn unit with bidentate carbonate	[99]
class c	([Tp′Zn(X)(Y)] with X and Y part of an anisobidentate (nitrate, carboxylate, etc.) ligand)	
31	$Tp^{tBu,Me}$Zn-methylcarbonate	[45]
32	$Tp^{Cum,Me}$Zn-dithiocarbonate	[46]
33	$Tp^{Cum,Me}$Zn-salicylate	[95]
34	Tp^{tBu}Zn-acetate	[100]
35	$Tp^{Cum,Me}$Zn-trifluoroacetate	[47]
36	$Tp^{tBu,Me}$Zn-thioacetate	[101]
37	$Tp^{Cum,Me}$Zn-dihydroorotate	[98]
38	Tp^{Ph}Zn-hydrogenmalonate	[102]
39	$Tp^{Cum,Me}$Zn-methylcarbonate	[46]
40	Tp^{Ph}Zn-cyanoacetate	[103]
41	$(Tp^{iPr,iPr}Zn)_2$-μ-carbonate, Zn unit with monodentate carbonate	[99]
42	$Tp^{Cum,Me}$Zn-γ-hydroxypropionate	[47]
43	$Tp^{Pic,Me}$Zn-acetate · $B(OH)_3$	[92]
44	Tp^{tBu}Zn-nitrate	[104]
45	Tp^{Ph}Zn-benzoate	[105]
46	Tp^{Ph}Zn-nitrate	[101]
47	Tp^{Ph}Zn-2-aminobenzoate	[94]
48	Tp^{Ph}Zn-benzylcarboxylate	[102]
49	TpZn-nitrate	[106]
class d	([Tp′Zn(X)(Y)] with one weakly coordinated Tp′ nitrogen)	
50	$Tp^{Ph,Me}$Zn-(ethyl)(nitrophenyl)phosphate · (3-methyl-5-phenylpyrazole)	[48]
51	$Tp^{Cum,Me}$Zn-(3-methyl-5-cumenylpyrazolide) · (3-methyl-5-cumenylpyrazole)	[107]
52	$Tp^{Cum,Me}$Zn-diphenylphosphate · (3-methyl-5-cumenylpyrazole)	[49]

0947-6539/99/0503-1024 $ 17.50+.50/0 *Chem. Eur. J.* **1999**, *5*, No. 3

the coordination polyhedra, and likewise those complexes in classes **a** and **b** containing Zn–S or Zn–I bonds became more the exception when treated with their real bond lengths.

Correlation between the two largest bond angles and the dihedral angle δ_{24}: In Figure 6, the two largest bond angles $\alpha1$ (angle 1–5) and $\alpha2$ (angle 2–4) of the 30 complexes have been plotted against the dihedral angle δ_{24}. The two curves describing the data for ideal complexes (with ideal = uniform bond lengths and symmetry C_{2v}) on the conventional Berry path are given as solid lines. For such complexes, the dihedral angle δ_{24} is a nonlinear function of $\alpha1$ and $\alpha2$, as given by Equation (8) in the main text and trigonometrically deduced in Figure 13. The two solid lines in Figure 6 have

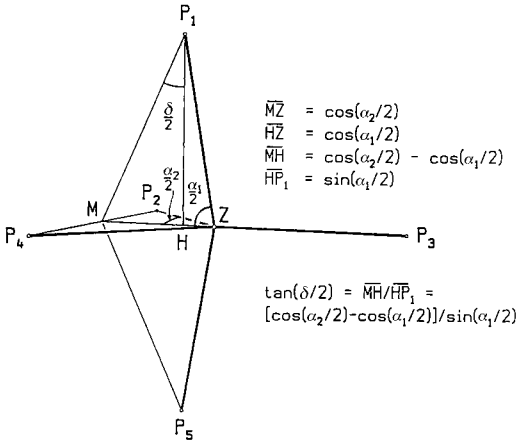

Figure 13. Angle definitions and trigonometrical correlations for the evaluation of Equation (8). All distances Z–P_n are assumed to be of unit length.

been calculated from Equation (8) under the assumption that $\alpha1 = 180 - \varepsilon$ and $\alpha2 = 120 + \varepsilon$ ($\varepsilon = 0$ to 30), which is consistent with a Berry rotation from a TBP to a SP with basal *trans* angles of 150°. In general, if the value of 150° is replaced by the variable p, the relationships expressed in Equations (10) and (11) are valid for $\alpha1$ and $\alpha2$. The pair of dotted lines in Figure 6 show the theoretical curves calculated for $p = 158°$.

$$\alpha1 = 180 - [(180 - p)/(p - 120)]\varepsilon \quad [\varepsilon = 0 \text{ to } (p - 120)] \tag{10}$$

$$\alpha2 = 120 + \varepsilon \tag{11}$$

Correlations between the complete sets of dihedral angles: Each bond angle in a ZnL_5 polyhedron defines an edge of the polyhedron, across which a characteristic dihedral angle between the two adjoining triangular faces exists. For the discussion of the correlations between these angles the above-mentioned labeling scheme is used (see Figure 14). The angles

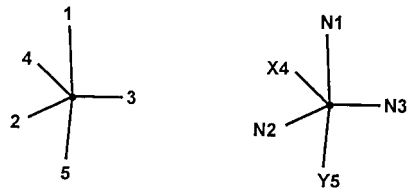

Figure 14. Orientation and labeling scheme for the ZnL_5 polyhedra.

resulting for the TBP and SP geometries are listed in Tables 7 and 8 (see below). For each dihedral angle δ in a TBP there is a corresponding dihedral angle δ in the corresponding SP. As first discussed by Muetterties,[81] the absolute differences between each two of these dihedral angles $|\delta_{TBP} - \delta_{SP}|$ can be summed up, yielding a quantitative measure of the TBP or SP character of the observed $[ML_5]$ complex as well as of the proximity of the $[ML_5]$ structure to the geometry defined by the Berry transition from ideal TBP to ideal SP. Specifically for the simplest case (i.e., unit bond lengths, ideal TBP defined by 180° and 120° bond angles, ideal SP defined by 150° and 105° bond angles) the value of $\Sigma|\delta_{TBP} - \delta_{SP}|$ is 217.7° and for each geometry between TBP and SP the value of $\Sigma(\Delta\delta_{TBP}) = \Sigma|\delta_{obs} - \delta_{TBP}|$ or $\Sigma(\Delta\delta_{SP}) = \Sigma|\delta_{obs} - \delta_{SP}|$ is smaller than 217.7°. The formulas for calculating the parameters (amount TBP) and (amount SP) in the range 0 to 1 from $\Sigma(\Delta\delta_{TBP})$ and $\Sigma(\Delta\delta_{SP})$ are given in the main text. If an observed structure of $[ML_5]$ adheres strictly to the Berry path, then $\Sigma(\Delta\delta_{TBP}) + \Sigma(\Delta\delta_{SP}) = 217.7°$, that is, (amount TBP) + (amount SP) = 1. For real $[ML_5]$ complex structures, this ideal correlation is not necessarily fulfilled exactly. In such a case we therefore calculate the averaged parameter $(\text{amount TBP})^{av}$ as a measure for the TBP character of a complex in the range 0 to 1 according to Equation (9) in the main text.

Table 7. Bond angles for ideal and adapted TBP and SP geometries.

	1–5	2–4	1–3	3–5	2–3	3–4	1–2	1–4	2–5	4–5
TBP(ideal)	180.0	120.0	90.0	90.0	120.0	120.0	90.0	90.0	90.0	90.0
TBP′(adapted)	169.5	129.8	87.0	86.2	100.0	129.8	87.0	100.5	86.2	90.0
SP(ideal)	150.0	150.0	105.0	105.0	105.0	105.0	86.2	86.2	86.2	86.2
SP′(adapted)	158.0	158.0	93.0	108.5	93.0	108.5	83.0	90.9	90.9	86.9

Table 8. Dihedral angles for ideal and adapted TBP and SP geometries (across the edges defined by the bond angles).

	1–5	2–4	1–3	3–5	2–3	3–4	1–2	1–4	2–5	4–5
TBP(ideal)	0.	53.1	101.5	101.5	53.1	53.1	101.5	101.5	101.5	101.5
TBP′(adapted)	0.	49.8	99.2	96.0	57.9	49.8	99.2	110.2	96.0	110.9
SP(ideal)	0.	0.0	76.9	76.9	76.9	76.9	118.5	118.5	118.5	118.5
SP′(adapted)	0.	0.0	77.2	73.3	77.2	73.3	114.7	119.8	119.8	127.1

Construction of the adapted $[ZnL_5]$ geometries TBP′ and SP′: The evaluations described so far are based on the geometries of simple unconstrained AB_5 species. However, the coordination geometries of our complexes differ systematically from these geometries (restraints induced by the Tp′ ligand and the fact that the basal *trans* angles of our SP measure 158° instead of 150°). To account for this, the geometries of the two prototypes, ideal TBP and SP, were modified to satisfy these obvious restraints, thus leading to the adapted complex geometries TBP′ and SP′ (Figure 15). The distortions to be applied were estimated by plausibility considerations; fine adjustment was performed by accounting for geo-

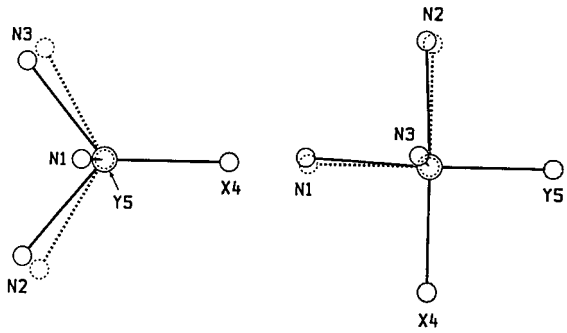

Figure 15. Adapted geometries TBP′ and SP′ (solid lines) superimposed on the ideal TBP and SP (dotted lines), each viewed along the main symmetry axis of TBP and SP.

metrical features or geometrical trends common to all the 30 complexes of the investigation. To this end, the 30 complexes first were sorted according to Figure 6, thus producing a series starting with the mostly TBP-like and ending with the mostly SP-like geometries. The modification $TBP_{ideal} \rightarrow TBP'$ was performed in three steps. First the two ligands N2 and N3 were rotated by 10° towards each other thus reducing the equatiorial angle N2-Zn-N3 to 100°, which is little more than the average value of the corresponding angles in the mostly TBP-like complexes (93° for SP-like complexes). In a second step, the axial ligand N1 was rotated by 4.7° about an axis lying in the (Zn, N2, N3) plane and being also perpendicular to the line Zn–X4. This reduced the angles N1-Zn-N2 and N1-Zn-N3 from 90° to 87°, which is about the average value of these angles in the mostly TBP-like complexes (83 and 93° for SP-like complexes). Note that in the series from the mostly SP-like complexes to the mostly TBP-like complexes the former angle is slightly increasing, while the latter is slightly decreasing such that 87° is the optimal value if both angles are considered

to be equal in the ideal modified structure. Finally, the whole (N1,N2,N3) fragment was rotated about the above-mentioned axis, such that all angles betwen the original positions of N1, N2, N3 and the final ones became equal (10.5°). The latter measure was due to the supposition that the restraints implied by the Tp′ geometry should affect the three corresponding ligand positions by an equal amount. The modification $SP_{ideal} \rightarrow SP'$ was performed in five steps. First, the two basal *trans* angles were increased to 158°. Then the two ligands N1, N2 were rotated by 2.5° about the pyramid axis, thus reducing the angle N1-Zn-N2 to 83°, which is the average value for this angle in the mostly SP-like complexes (85° for TBP-like complexes). In a third step, the ligand N3 was rotated by 10.8° about an axis perpendicular to the original pyramid axis, such that the angles N1-Zn-N3 and N2-Zn-N3 (101° in the original SP) were reduced to 93°, which also is the average value of these angles in the mostly SP-like complexes. In a fourth step, the whole (N1,N2,N3) fragment was rotated about this latter axis such that all angles between the original positions of N1, N2, N3 and the final ones became equal (7.1° in this case, see above). Finally the basal *trans* angles, which had grown to 160° by the last measure, were readjusted to 158° by rotating X and Y correspondingly. TBP′ as well as SP′ are defined to have C_m symmetry (cf. Figure 15), but as the mirror plane is oriented differently in the two complexes all complexes lying between them on the modified Berry path should have symmetry C_1. The value of $\Sigma\,|\,\delta_{TBP'} - \delta_{SP'}\,|$, that is, the sum of all absolute differences between the corresponding dihedral angles, is 202.3° for this adjusted TBP′/SP′ pair as compared to 217.7° for the ideal TBP/SP pair. Therefore, the value of 217.7 has to be replaced by 202.3 in calculating parameters like (amount TBP′). It should be noted that the straight lines in Figures 7 and 8 probably have the function of border lines for the data points. Points on the straight line represent complexes that correspond to the minimal sum $\Sigma\Delta\delta_{SP} + \Sigma\Delta\delta_{TBP} = p$ (with $p = 217.7$ or 202.3°). For points below the line, this sum would calculate less than minimal, which should be impossible. Thus, by definition the data points in Figures 7 and 8 should always lie on or above the lines. Table 7 lists the bond angles defined by the idealized coordination geometries discussed above, and Table 8 lists the corresponding dihedral angles.

Evaluations: According to the procedures outlined above, the calculated dihedral angle sums and the values of (amount TBP) and so on are tabulated in Table 9 for the 30 [Tp′Zn(X)(Y)] complexes in classes **a** and **b**.

Table 9. Dihedral angle sums and values of (amount TBP).

	Σ_{T1}[a]	Σ_{P1}[b]	V1[c]	Σ_{T2}[d]	Σ_{P2}[e]	V2[f]	V3[g]
1	92.5	92.5	0.58	69.6	69.6	0.66	0.53
2	78.2	46.1	0.71	34.1	23.3	0.86	0.75
3	131.0	126.8	0.41	108.1	108.1	0.47	0.39
4	119.5	119.5	0.45	96.6	96.6	0.52	0.43
5	85.2	80.0	0.62	57.2	57.2	0.72	0.63
6	52.4	30.5	0.81	8.4	7.7	0.96	0.61
7	77.5	76.5	0.65	53.7	53.7	0.73	0.58
8	73.7	69.3	0.67	49.3	46.5	0.76	0.64
9	69.2	69.2	0.68	52.1	46.3	0.76	0.58
10	60.4	50.1	0.75	27.2	27.2	0.87	0.61
11	59.0	53.9	0.74	46.1	31.1	0.81	0.45
12	117.2	117.2	0.46	94.4	94.4	0.53	0.35
13	113.9	113.9	0.48	91.1	91.1	0.55	0.46
14	125.1	123.4	0.43	102.3	102.3	0.49	0.42
15	81.6	63.9	0.67	41.8	41.0	0.80	0.69
16	79.4	50.9	0.70	37.7	28.0	0.84	0.77
17	56.4	37.3	0.78	17.4	14.4	0.92	0.59
18	62.9	56.1	0.73	34.2	33.3	0.83	0.53
19	59.5	48.1	0.75	25.2	25.2	0.88	0.65
20	62.2	48.5	0.75	26.7	25.7	0.87	0.62
21	172.2	159.0	0.24	149.4	149.4	0.26	0.21
22	170.7	159.5	0.24	147.8	147.8	0.27	0.22
23	148.3	140.1	0.34	125.4	125.4	0.38	0.30
24	94.0	91.8	0.57	69.1	69.1	0.66	0.57
25	87.8	58.7	0.66	43.8	36.4	0.80	0.69
26	89.4	47.7	0.69	45.7	24.8	0.83	0.78
27	104.3	98.5	0.53	80.6	80.6	0.60	0.50
28	68.7	52.7	0.72	33.9	29.9	0.84	0.67
29	112.5	87.6	0.54	72.7	71.5	0.64	0.52
30	120.2	50.9	0.61	75.0	38.7	0.72	0.51

[a] $\Sigma_{T1} = \Sigma\,|\,\delta_{obs} - \delta_{TBP}\,|$ for perfect TBP. [b] $\Sigma_{P1} = 217.7 - \Sigma\,|\,\delta_{obs} - \delta_{SP}\,|$ for perfect SP. [c] V1 = (amount TBP)[av]. [d] $\Sigma_{T2} = \Sigma\,|\,\delta_{obs} - \delta_{TBP'}\,|$ for adapted TBP′ (see above). [e] $\Sigma_{P2} = 202.3 - \Sigma\,|\,\delta_{obs} - \delta_{SP'}\,|$ for adapted SP′ (see above). [f] V2 = (amount TBP′)[av]. [g] V3 = (amount TBP) calculated from [(angle 1–5) – (angle 2–4)] / 60, cf. Reedijk et al.[83]

Acknowledgments

This work was supported by the Deutsche Forschungsgemeinschaft and the Fonds der Chemischen Industrie.

[1] M. F. Dunn, *Struct. Bonding (Berlin)* **1975**, *23*, 61–122.
[2] R. S. Brown, J. Huguet, N. J. Curtis, in *Zinc and its Role in Biology and Nutrition* (Ed.: H. Sigel), Marcel Dekker, New York, **1983**, pp. 55–99.
[3] R. H. Prince, in *Comprehensive Coordination Chemistry*, *Vol. 5* (Eds.: G. Wilkinson, R. D. Gillard, J. A. McCleverty), Pergamon, Oxford, **1987**, pp. 925–1045.
[4] D. E. Fenton, H. Okawa, *J. Chem. Soc. Dalton Trans.* **1993**, 1349; D. E. Fenton, H. Okawa, *Chem. Ber.* **1997**, *130*, 433.
[5] E. Kimura, *Prog. Inorg. Chem.* **1994**, *41*, 443; E. Kimura, T. Koike, *Adv. Inorg. Chem.* **1997**, *44*, 229.
[6] H. Vahrenkamp, in *Bioinorganic Chemistry – Transition Metals in Biology and their Coordination Chemistry* (Ed.: A. X. Trautwein), Wiley-VCH, Weinheim, **1997**, pp. 540–551.
[7] *Zinc Enzymes* (Ed.: T. G. Spiro), Wiley, New York, **1983**.
[8] *Zinc and its Role in Biology and Nutrition* (Ed.: H. Sigel), Marcel Dekker, New York, **1983**.
[9] *Zinc Enzymes* (Eds.: I. Bertini, C. Luchinat, W. Maret, M. Zeppezauer), Birkhäuser, Boston, **1986**.
[10] B. L. Vallee, D. S. Auld, *Acc. Chem. Res.* **1993**, *26*, 543, and references therein.
[11] D. W. Christianson, *Adv. Protein Chem.* **1991**, *42*, 281.
[12] J. E. Coleman, P. Gettins, *Adv. Enzymol.* **1983**, *55*, 381.
[13] E. Kimura, T. Shiota, T. Koike, M. Shiro, M. Kodama, *J. Am. Chem. Soc.* **1990**, *112*, 5805.
[14] R. Alsfasser, S. Trofimenko, A. Looney, G. Parkin, H. Vahrenkamp, *Inorg. Chem.* **1991**, *30*, 4098.
[15] S. Hikichi, M. Tanaka, Y. Moro-oka, N. Kitajima, *J. Chem. Soc. Chem. Commun.* **1992**, 814.
[16] M. Ruf, K. Weis, H. Vahrenkamp, *J. Chem. Soc. Chem. Commun.* **1994**, 135.
[17] C. Kimblin, W. E. Allen, G. Parkin, *J. Chem. Soc. Chem. Commun.* **1995**, 1813.
[18] M. Ruf, R. Burth, K. Weis, H. Vahrenkamp, *Chem. Ber.* **1996**, *129*, 1251.
[19] K. Weis, H. Vahrenkamp, *Inorg. Chem.* **1997**, *36*, 5592.
[20] P. Wooley, *Nature* **1975**, *258*, 677. P. Wooley, *J. Chem. Soc. Perkin Trans. 2* **1977**, 318.
[21] I. Tabushi, Y. Kuroda, A. Mochizuki, *J. Am. Chem. Soc.* **1980**, *102*, 1152.
[22] R. S. Brown, N. J.Curtis, J. Huguet, *J. Am. Chem. Soc.* **1981**, *103*, 6953.
[23] M. Kato, T. Ito, *Inorg. Chem.* **1985**, *24*, 504.
[24] N. N. Murthy, K. D. Karlin, *J. Chem. Soc. Chem. Commun.* **1993**, 1236.
[25] D. S. Sigman, C. T. Jorgensen, *J. Am. Chem. Soc.* **1972**, *94*, 1724.
[26] J. Chin, X. Zuo, *J. Am. Chem. Soc.* **1984**, *106*, 3687.
[27] J. Suh, O. Han, B. Chang, *J. Am. Chem. Soc.* **1986**, *108*, 1839.
[28] J. T. Groves, R. M. Dias, *J. Am. Chem. Soc.* **1979**, *101*, 1033.
[29] T. H. Fife, V. L. Squillacote, *J. Am. Chem. Soc.* **1978**, *100*, 4787.
[30] N. Sträter, W. N.Lipscomb, T. Klabunde, B. Krebs, *Angew. Chem.* **1996**, *108*, 2158; *Angew. Chem. Int. Ed. Engl.* **1996**, *35*, 2024.
[31] C. Bazzicalupi, A. Bencini, A. Bianchi, V. Fusi, C. Giorgi, P. Paoletti, B. Valtancoli, D. Zanchi, *Inorg. Chem.* **1997**, *36*, 2784.
[32] W. H. Chapman, R. Breslow, *J. Am. Chem. Soc.* **1995**, *117*, 5462.
[33] T. A. Bruice, A. Tsubouchi, R. O. Dempcy, L. P. Olson, *J. Am. Chem. Soc.* **1996**, *118*, 9867.
[34] T. Koike, M. Inoue, E. Kimura, M. Shiro, *J. Am. Chem. Soc.* **1996**, *118*, 3091.

0947-6539/99/0503-1026 $ 17.50+.50/0 *Chem. Eur. J.* **1999**, *5*, No. 3

[35] V. Scheller-Krattiger, H. Sigel, *Inorg. Chem.* **1986**, *25*, 2628.
[36] H. Sigel, *Chem. Soc. Rev.* **1993**, *22*, 255.
[37] S. H. Gellman, R. Petter, R. Breslow, *J. Am. Chem. Soc.* **1986**, *108*, 2388.
[38] P. R. Norman, *Inorg. Chim. Acta* **1987**, *130*, 1; P. R. Norman, A. Tate, P. Rich, *Inorg. Chim. Acta* **1988**, *145*, 211.
[39] T. Koike, E. Kimura, *J. Am. Chem. Soc.* **1991**, *113*, 8935.
[40] Y. Fujii, T. Itoh, K. Onodera, T. Tada, *Chem. Lett.* **1995**, 305; T. Itoh, Y. Fujii, T. Tada, Y. Yoshikawa, H. Hisada, *Bull. Chem. Soc. Jpn.* **1996**, *69*, 1265.
[41] H. Adams, N. A. Bailey, D. E. Fenton, Q. Y. He, *J. Chem. Soc. Dalton Trans.* **1996**, 2857.
[42] O. Tapia, O. Jacob, F. Colonna, *Theor. Chim. Acta* **1993**, *85*, 217.
[43] K. M. Merz, L. Banci, *J. Am. Chem. Soc.* **1997**, *119*, 863.
[44] M. Ruf, K. Weis, H. Vahrenkamp, *J. Am Chem. Soc.* **1996**, *118*, 9288.
[45] R. Alsfasser, M. Ruf, S. Trofimenko, H. Vahrenkamp, *Chem. Ber.* **1993**, *126*, 703.
[46] M. Ruf, H. Vahrenkamp, *Inorg. Chem.* **1996**, *35*, 6571.
[47] M. Ruf, H. Vahrenkamp, *Chem. Ber.* **1996**, *129*, 1025.
[48] K. Weis, M. Rombach, M. Ruf, H. Vahrenkamp, *Eur. J. Inorg. Chem.* **1998**, 263.
[49] K. Weis, H. Vahrenkamp, *Eur. J. Inorg. Chem.* **1998**, 271.
[50] K. Weis, M. Rombach, H. Vahrenkamp, *Inorg. Chem.* **1998**, *37*, 2470.
[51] R. Walz, K. Weis, M. Ruf, H. Vahrenkamp, *Chem. Ber.* **1997**, *130*, 975.
[52] M. Ruf, F. A. Schell, R. Walz, H. Vahrenkamp, *Chem. Ber.* **1997**, *130*, 101.
[53] C. Blindauer, H. Vahrenkamp, unpublished results.
[54] V. E. Bel'skii, L. A. Kydryavtseva, O. M. Il'ina, B. E. Ivanov, *J. Gen. Chem. USSR (Engl. Transl.)* **1979**, 2180; H. Waeschke, R. Mitzner, *Z. Chem.* **1980**, *20*, 381.
[55] J. R. Cox, O. B. Ramsay, *Chem. Rev.* **1964**, *64*, 317; A. J. Kirby, S. G. Warren, *The Organic Chemistry of Phosphorus*, Elsevier, Amsterdam, **1967**.
[56] R. Clewley, H. Slebocka-Tilk, R. S. Brown, *Inorg. Chim. Acta* **1989**, *157*, 233.
[57] I. O. Kady, B. Tan, Z. Ho, T. Scarborough, *J. Chem. Soc. Chem. Commun.* **1995**, 1137; E. Kimura, Y. Kodama, T. Koike, M. Shiro, *J. Am. Chem. Soc.* **1995**, *117*, 8304.
[58] D. Wahnon, A.-M. Lebuis, J. Chin, *Angew. Chem.* **1995**, *107*, 2594; *Angew. Chem. Int. Ed. Engl.* **1995**, *34*, 2412.
[59] a) R. G. Wilkins, *Kinetics and Mechanism of Reactions of Transition Metal Complexes*, 2nd ed., VCH, Weinheim, **1972**; b) A. J. Kirby, in *Comprehensive Chemical Kinetics*, *Vol. 11* (Eds.: C. H. Bamford, C. F. H. Tipper), Elsevier, New York, **1969**, pp. 57–208.
[60] N. Isaacs, *Physical Organic Chemistry*, 2nd ed., Longman, Harlow, **1995**, pp. 507–519.
[61] M. S. Janssen, in *The chemistry of carboxylic acids and esters* (Ed.: S. Patai), Wiley-Interscience, New York, **1969**, pp. 730–735.
[62] J. Chin, *Acc. Chem. Res.* **1991**, *24*, 145, and references therein.
[63] B. Zhang, R. Breslow, *J. Am. Chem. Soc.* **1997**, *119*, 1676, and data cited therein.
[64] R. S. Brown, M. Zamkanei, J. L. Cocho, *J. Am. Chem. Soc.* **1984**, *106*, 5222.
[65] T. Koike, S. Kajitani, I. Nakamura, E. Kimura, M. Shiro *J. Am. Chem. Soc.* **1995**, *117*, 1210, and references therein.
[66] S. Zhu, W. Chen, H. Lin, X. Yiu, F. Kou, M. Lin, Y. Chen, *Polyhedron* **1997**, *16*, 3285.
[67] C. Wendelstorf, S. Warzeska, E. Kövari, R. Krämer, *J. Chem. Soc. Dalton Trans.* **1996**, 3087.
[68] E. Kimura, I. Nakamura, T. Koike, M. Shionoya, Y. Kodama, T. Ikeda, M. Shiro, *J. Am. Chem. Soc.* **1994**, *116*, 4764.
[69] T. Koike, M. Takamura, E. Kimura, *J. Am. Chem. Soc.* **1994**, *116*, 8443.
[70] M. C. Favas, D. L. Kepert, *Prog. Inorg. Chem.* **1980**, *27*, 325.
[71] S. Trofimenko, *Chem. Rev.* **1993**, *93*, 943.
[72] G.Parkin, *Adv. Inorg. Chem.* **1996**, *42*, 291.
[73] N. Kitajima, W. B. Tolman, *Prog. Inorg. Chem.* **1995**, *43*, 419.
[74] H. B. Bürgi, J. D. Dunitz, *Acc. Chem. Res.* **1983**, *16*, 153.
[75] A. G. Orpen, *Chem. Soc. Rev.* **1993**, *22*, 191.
[76] B. F. G. Johnson, Y. V. Roberts, E. Parisini, R. E. Benfield, *J. Organomet. Chem.* **1994**, *478*, 218.
[77] D. Braga, F. Grepioni, K. Biradha, G. R. Desiraju, *J. Chem. Soc. Dalton Trans.* **1996**, 3925.
[78] T. P. E. Auf der Heyde, *Angew. Chem.* **1994**, *106*, 871; *Angew. Chem. Int. Ed. Engl.* **1994**, *33*, 823.
[79] J. M. Smith, N. Coville, *Organometallics* **1996**, *15*, 3388.
[80] T. P. E. Auf der Heyde, L. R. Nassimbeni, *Acta Crystallogr. Sect. B* **1984**, *40*, 582.
[81] E. L. Muetterties, L. J. Guggenberger, *J. Am. Chem. Soc.* **1974**, *96*, 1748.
[82] R. R. Holmes, *Acc. Chem. Res.* **1979**, *12*, 257.
[83] A. W. Addison, T. N. Rao, J. Reedijk, J. van Rijn, G. C. Verschoor, *J. Chem. Soc. Dalton Trans.* **1984**, 1349.
[84] The observation that all points deviating from the Berry line are positioned only above this line is discussed in detail in the Structure Correlation section.
[85] All geometrical calculations as well as all drawings of molecular structures were done with an enhanced version of the computer program SCHAKAL 97.[86]
[86] E. Keller, SCHAKAL 97, a computer program for the graphical representation of molecular and crystallographic models, Universität Freiburg, **1997**.
[87] M. Ruf, K. Weis, I. Brasack, H. Vahrenkamp, *Inorg. Chim. Acta* **1996**, *250*, 271.
[88] N.-Y. Chang, C. Lim, *J. Am. Chem. Soc.* **1998**, *120*, 2156.
[89] E. L. Eliel, S. H. Wilen, L. N. Mander, *Stereochemistry of Organic Compounds*, Wiley, New York, **1994**, pp. 876–880.
[90] P. W. Atkins, *Physical Chemistry*, 5th ed., Oxford University Press, Oxford, **1994**, p. 875.
[91] T. Brandsch, F. A. Schell, K. Weis, M. Ruf, B. Müller, H. Vahrenkamp, *Chem. Ber.* **1997**, *130*, 283.
[92] K. Weis, Dissertation, Universität Freiburg, **1997**.
[93] R. Walz, Dissertation, Universität Freiburg, **1998**.
[94] A. Kremer-Aach, W. Kläui, R. Bell, A. Strerath, H. Wunderlich, D. Mootz, *Inorg. Chem.* **1997**, *36*, 1552.
[95] U. Hartmann, H. Vahrenkamp, *Chem. Ber.* **1994**, *127*, 2381.
[96] M. Ruf, B. C. Noll, M. Groner, G. T. Yee, C. G. Pierpont, *Inorg. Chem.* **1997**, *36*, 4860.
[97] M. Ruf, A. M. Lawrence, B. C. Noll, C. G. Pierpont, *Inorg. Chem.* **1998**, *37*, 1992.
[98] M. Ruf, K. Weis, H. Vahrenkamp, *Inorg. Chem.* **1997**, *36*, 2130.
[99] N. Kitajima, S. Hikichi, M. Tanaka, Y. Moro-oka, *J. Am. Chem. Soc.* **1993**, *115*, 5496.
[100] A. Looney, R. Han, I. B. Gorell, M. Cornebise, K. Yoon, G. Parkin, A. L. Rheingold, *Organometallics* **1995**, *14*, 274.
[101] R. Alsfasser, A. K. Powell, S. Trofimenko, H. Vahrenkamp, *Chem. Ber.* **1993**, *126*, 685.
[102] D. J. Darensbourg, M. W. Holtcamp, B. Khandelwal, K. K. Klausmeyer, J. H. Reibenspies, *Inorg. Chem.* **1995**, *34*, 2389.
[103] D. J. Darensbourg, M. W. Holtcamp, E. M. Longridge, B. Khandelwal, K. K. Klausmeyer, J. H. Reibenspies, *J. Am. Chem. Soc.* **1995**, *117*, 318.
[104] R. Han, G. Parkin, *J. Am. Chem. Soc.* **1991**, *113*, 9707.
[105] S. Kawabata, N. Nakata, K. Ichikawa, *Acta Crystallogr. Sect. C* **1995**, *51*, 1554.
[106] A. Looney, G. Parkin, *Inorg. Chem.* **1994**, *33*, 1234.
[107] M. Ruf, Dissertation, Universität Freiburg, **1996**.

Received: September 16, 1998 [F1349]